École polytechnique de Louvain

Reducing the variability of renewable energy systems

Evaluation of the robustness of typical energy systems

Authors: **Edouard COLLING, Yassine KOURAICHI**
Supervisors: **Fransesco CONTINO, Diederik COPPITTERS**
Reader: **Gauthier LIMPENS**
Academic year 2020–2021
Master [120] in Electro-mechanical Engineering

Abstract

Our current energy system is shifting from fuel-powered and centralised power generation to small-scaled renewable architectures. However, modelling such energetic crossroad includes many uncertainties as renewable energy sources are likely subject to intermittency and lack of knowledge due to their recent emergence. This master thesis performs robust design optimization analysis for various energetic scenarios including renewable technologies. The task consists in enhancing the economical robustness of an energy system made of photovoltaic arrays and battery storage. *Economical robustness* in an energetic context is the propensity to predict accurately the cost of an energetic system, with parameters that could variate (solar irradiance, cost of technologies, demand fluctuations). In other words, the optimal profile of the investigated system should both minimize the cost of it and its stochastic variation caused by uncertain parameters.
Robust design optimization of the basic PV-Battery system will be implemented by adding three technologies (micro gas turbine, internal combustion engine, heat pump unit) likely to enhance the economical prediction accuracy of the whole system while satisfying both heat and electrical demands. The duality of demand leads to minimize the Levelized Cost of eXergy for all couplings. Moreover, for each subsystem, uncertainty quantification has been applied to determine how the uncertain parameters are stochastically represented.
For all the pairings and various scenarios, the impact of uncertainties on the stochastic output have been quantified. Moreover, the optimized system configurations to lower the mean cost or to provide robustness are known.

Key words: Robust Design Optimization, Energy Systems Models, Multi-Objective Optimization, Uncertainty Quantification, LCOX Minimization.

Acknowledgments

"We would like to thank the following people without whom the realization of this work and its success would not have been possible!

Thank you Professor Francesco Contino, supervisor of this master thesis, who gave us the opportunity to work on a stimulating subject, introduced by himself earlier in the year as part of a inspiring lecture.

Special thanks to Diederik Coppiters (PhD candidate at VUB), our mentor. Behold his regular availability and precious feedbacks, Diederik guided us to professionalize a research. The rigour he taught us will surely be an asset in the future.

We wanted to thanks Gauthier Limpens (PhD candidate at UCLouvain), jury member, for being part of our last project at university. His enthusiasm and professionalism were truly appreciated throughout our study years for several projects he supervised.

Finally, special mention to our parents for all the support, their education and the opportunity to learn they gave us.

Yassine & Edouard."

Computational resources have been provided by the supercomputing facilities of the Université catholique de Louvain (CISM/UCL) and the Consortium des Équipements de Calcul Intensif en Fédération Wallonie Bruxelles (CÉCI) funded by the Fonds de la Recherche Scientifique de Belgique (F.R.S.-FNRS) under convention 2.5020.11 and by the Walloon Region.

Contents

List of Figures

Nomenclature

$\boldsymbol{\eta}$ efficiency

$\boldsymbol{\mu}$ mean

$\boldsymbol{\phi}$ orthogonal polynomial

$\boldsymbol{\sigma}$ standard deviation

$\boldsymbol{\xi}$ vector of uncertain parameters

AC Alternating Current

bat battery

$\mathbf{C}_{e,a}$ annual grid electricity cost

$\mathbf{C}_{g,a}$ annual gas cost

$\mathbf{C}_{r,a}$ annual replacement cost

$\mathbf{CAPEX}_a$ annual capital expense, €

CAPEX capital expense, €$/kW$

CC Combustion Chamber

CHP Combined Heat and Power

DC Direct Current

DV(s) Design variable(s)

E Energy

F Carnot Factor

HP Heat Pump

ICE Internal Combustion Engine

I Current

LCOX Levelized Cost Of eXergy, €$/kWh$

MGT Micro Gas Turbine

NSGA-II Non-Dominated Sorting Genetic Algorithm 2

n system capacity

O&M Operation & Maintenance

OPEX$_a$ annual operational cost; €

OPEX operational cost, €$/kWh$

PCE Polynimial Chaos Expansion

PMC Power Module Controller

PV PhotoVoltaic

P Power

Q Heat

RDO Robust Design Optimization

R Resistance

SOC State Of Charge

std standard deviation

s entropy

TSO Transmission System Operator

T Temperature

UQ Uncertainty Quantification

U Voltage

V$_{rms}$ root mean square voltage

X eXergy

Chapter 1

Introduction

1.1 Energetic context in Belgium and solar potential

Ensuring energetic ecological transition is one of the major challenge for the current engineering generation. The global world is concerned by climate change and their consequences are already perceptible. Individual CO_2-emissions are rising, mostly in developing or rich countries. In 2018, the global energy-related emissions of carbone dioxyde rose up to an historic amount of 33 GT. Asian countries and USA account for 85% of this trend, mostly from coal power plants [1]. As energy use (residential, transport and industry) amount to 75% [2] of the global world emissions, the development of renewable energies is a priority if we want to avoid irreversible damages.

Up to 46% of the Belgian electricity production relies on nuclear energy. However, for safety reasons, authorities have decided to close all nuclear facilities by the year 2025. In order to keep ecological targets and ensure stability, this loss should largely be compensated with renewables (up to 50% of it [3]).

To achieve renewable transition, solar energy is likely to be the most suitable source. Solar technology is getting more efficient and cheaper over the years. It is even presumed that its cost will be divided by two over the next decade. It is even expected that its cost will be halved over the next decade and that the price of battery systems will decrease by 40% between 2020 and 2030 [4]. Coupled to batteries that address solar fluctuations, this high-potential technology is likely to dominate the energetic landscape in the coming years and to be the production technology for the transition.

However, such PV-battery systems are facing much impactful uncertainties on several parameters (e.g., technology costs) and because of solar intermittency, they do not offer a robust solution. "Robust" term means that for a non-deterministic deployment facing the related uncertain parameters, it can be stated with more or less confidence that it may fulfill the demand properly at a certain cost of investment. To enhance the robustness of such systems, the task consists in developing models where this promising couple is working alongside with another (co-)generation subsystem. Three coupling solutions will be implemented: micro-gas turbine, piston engine and heat-pump. As you may notice, the three subsystems are able to provide heat energy. Indeed, this master thesis will address both electrical and heat demands and apply robust analysis to the three options.

1.2 Master thesis objective: Robust Design Optimization

The goal of optimization is to determine the best set of variables to meet one or several objectives. In an energetic context, the objectives can vary widely (e.g., cost minimization, self-sufficiency maximization, failures risks minimization). As far as this master thesis is concerned, the objective of interest is cost minimization and the set of variables that shaped the model are the power of the energetic installations that sustain the system (e.g., solar panel peak power, battery stacks capacity, third system nominal power).

To perform optimization, a numerically shaped energetic model is needed. It will depend on parameters such as solar irradiance, daily demand in electricity and heat or costs of the various technologies. Such parameters are fluctuating all the time and current values could widely variate over decades or even years. For example, the price of electricity in Belgium is expected to rise sharply after nuclear decommissioning. Therefore, a deterministic optimization of an energetic model could not help to design accurate plans on the future as real life is non-deterministic. So-called *robust optimization* will take the uncertainty of parameters into account. It estimates how much the uncertainties weigh in the balance through *Sobol indices*, explores and shapes a probabilistic curve of the objectives.

The objective of this master thesis is to build and interprete accurate eco-friendly **production** models using robust optimization. Robust designs and their interpretations can enhance trust in promising green technologies.

1.3 Contents

The first chapter of the work is an introduction to the world of robust design optimization.
The global energetic model will then be explained. It will show how the demand is represented and how technologies are interacting with each others. A first robust

optimization analysis on a basic system is carried out to contextualize the aim of the work.
Afterwards, the three subsystems will be analysed separately. First, the technologies will be re-explained and the assumptions made to model them will be discussed. Finally, RDO results for each subsystem coupling will be exposed and interpreted.

Chapter 2

Robust optimisation of energy systems

As said previously, the goal of robust design optimization (RDO) is to shape a stochastic distribution of the optimization's objectives, taking uncertainties of parameters into account. This chapter will get you more familiar with the method and uncertainties.

2.1 Parameters and uncertainties

2.1.1 What is an uncertainty? An uncertain parameter?

An uncertain parameter is simply an element of the model that may variate over time due to natural variation or imprecision on its value. An uncertainty of a parameter can be **natural** or **epistemic**.

Natural uncertainty

To illustrate a natural uncertainty, let's take the example of intermittent solar irradiance, useful to evaluate photovoltaic panels potential. Holding irradiance data from past years may give an idea of how it may fluctuate but in reality, one could face series of brighter/darker days at aleatory moment of the year. In other words, the solar irradiance is a parameter that naturally variate (clouds, humidity rate) and precise knowledge on previous variations can not reduce the uncertainty on it.

Epistemic uncertainty

At the opposite of natural uncertainty, deeper knowledge and study on the parameter may help to reduce an epistemic uncertainty. As an example, it is expected that the cost of solar panels (in [$€/kW_{peak}$]) will decrease in the upcoming decades [5]. It thus involves an uncertainty on this parameter. The evolution of the price can be anticipated via researches and the uncertainty on it can be reduced by collecting more data. Even more, the range could be reduced in the future as those fluctuations are actually faced and thus the previous estimation of the range could be re-evaluated.

2.1.2 Representation of uncertainty and impact on model parameters

An uncertain parameter is stochastically quantified by a mean, a variance and a distribution. In this study, for simplification reasons, the uncertainties are always represented as an uniform probability density function, around an average value and a variance. The variance expresses the wideness of the range. The mean value is thus not the actual value for the data, it is the middle value of the range of possibilities. Two different cases must be considered.

Horizontal shape, variable range

Type of parameter: when the value of the parameter can be fixed between two points and may worth uniformly between them.
Distribution: uniform probability curve
Mean: middle value.
Variance: fix the wideness around the mean.
As an example, the cost of pv-panels ($CAPEX$) is uniformly distributed around 605 [€/kWh_{peak}] with a variance of 175. It means that the cost could be between 430 (605-175) and 780 (605+175) [€/kWh_{peak}].

Specific shape, variable height

Type of parameter: when the value of the parameter follows a familiar style and could not naturally fluctuate uniformly between two extreme values (demand profile, solar irradiance, temperature)
Distribution: specific probability curve
Mean: middle value of height variation of the curve.
Variance: half the range of height variation.

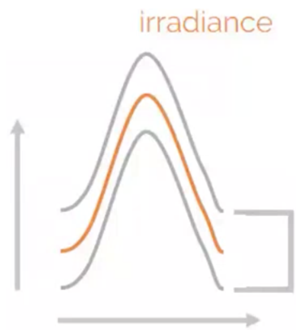

2.1.3 Stochastic quantification of uncertainties

The uncertainty quantification methods used for the aim of this work depend on the studied parameters. For some of them, documents and literature on energy transitions helped to characterize the potential evolution of some parameters (Source Elia: [6]).

Much inspiration has been taken from the works of master thesis supervisor, Diederik Coppitters[1]. The RDO-tools that he and his colleagues have developed were strong basis for this master thesis. For the parameters proper to the 3 coupled subsystems (micro-gas turbine, piston engine, variable speed heat pump), specific uncertainty quantification has been done to fix their stochastic range. parameters. The method used is to spot the extreme values that the parameters may have or have had in the past and to simply draw an uniform probability distribution between them.

2.2 Whole RDO-method described

RDO is based on the elaboration of a simplified surrogate model to represent a complex system. In fact, the energetic model representing the energy system is computationally complex, with much parameters subject to uncertainties. To optimize the technological set-up and minimizing its cost, thousands of runs should be completed and thus, a simplified surrogate model, approaching the real model is an asset. The following figure(2.1) illustrates the consecutive which lead to the development of one surrogate model, using Polynomial Chaos Expansion method (PCE). The consecutive steps and their connections will be detailed one by one afterwards.

As *RDO* goal is to *optimize* the objective function with a robustness evaluation, let's redefine the terms "design variables", "objectives"...

The **objectives** is the values of the function targeted by the optimization. It can be both minimization or maximization on outputs such as example *Levelized cost of exergy* ("real" cost of thermal and electric energy system) and *self-sufficiency ratio* (ability of a system to work independently from the grid).
The **design variables** are the numerical inputs that are changed by the optimizer itself to explore the different panels of results. It allows the optimizer to find the best coordination of them to meet the objectives.

As parameters of the model are stochastic, the outputs will also be ranged stochastically. Thus, those outputs will be characterized by a mean and a variance. RDO objectives are the minimization of both LCOX mean value and variance. The minimization of the mean is equivalent to pure optimization of price while the minimization of variance provides robustness on its prediction. The upcoming chapters will illustrate and explain the trade-offs between each objective. Now, let's

[1]https://scholar.google.be/citations?user=G91ATvgAAAAJhl=nl

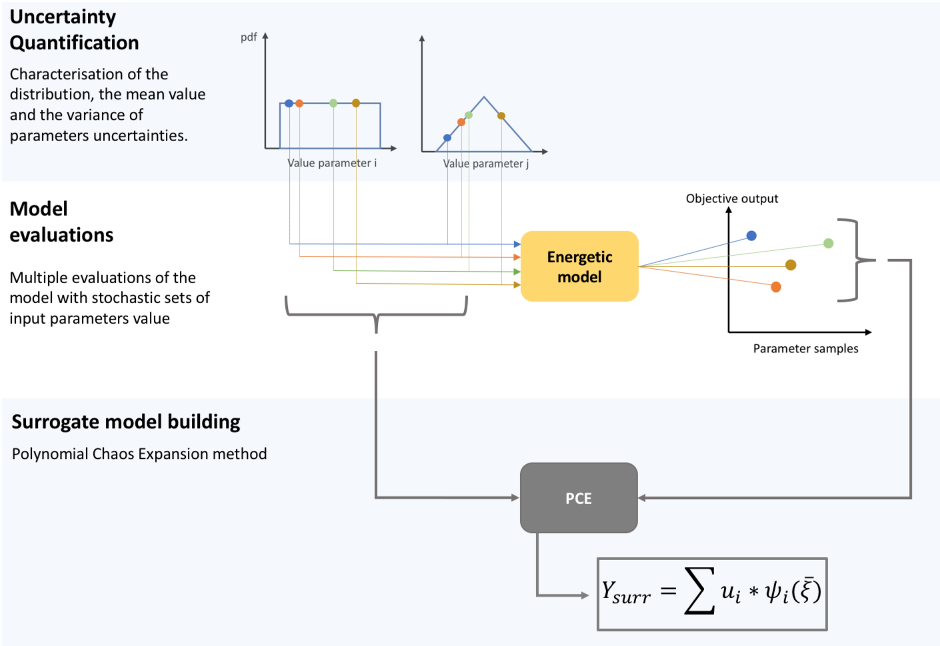

Figure 2.1: Surrogate model development via PCE method: first step is the **Uncertainty quantification**. It consists in the stochastic characterisation of the parameters that could variate within the model. Then, a multitude of **model evaluations** are performed, with large variety of uncertain parameters values associations. It maps the LCOX outputs for different values combinations. The building of the surrogate model is then ensured by the **Polynomial Chaos Expansion** method, linking the sets of uncertainty values and the LCOX mapping of the previous step. The approach of the real model is done by a weighted sum of orthogonal polynomial functions, taking the uncertain parameters in input.

dive more into "RDO black box".

2.2.1 Uncertainty characterisation

This step designs the uncertainties on parameters as probability density functions. For each of those, the distribution, the mean value and the variance have to be dressed down in a repertory. The characterisation of the uncertainties is a crucial step as the aim of *RDO* is to explores design possibilities and quantify the impact of uncertainties on optimization objectives.

2.2.2 Model evaluations

The interaction between parameters is managed by an energetic model developed in Python. The supplies of technologies and exchanges of energies are handled there. The whole model will be deeply described in the next chapters.

What concerns *RDO*, numerous model evaluations are performed to explore the various responds depending on parameters configuration. In other words, the model run for multiple set-ups of parameters subjected to uncertainties and map the outputs.

2.2.3 Uncertainties propagation: Polynomial Chaos Expansion

Polynomial chaos expansion (*PCE*) interpretes the various deterministic outputs from the previous step to build a surrogate model of the whole energetic system. This surrogate model $\hat{Y}$ approaches the real one as a sum of orthogonal polynomial functions taking a vector of uncertain parameters ($\boldsymbol{\xi}$) in input [7]. Considering the number of uncertainties and the computational cost, a simplified mathematical model can be elaborated thanks to this truncated scheme.

$$Y(\boldsymbol{\xi}) \simeq \hat{Y}(\boldsymbol{\xi}) = \sum_{i=0}^{P} \hat{u}_i \psi_i(\boldsymbol{\xi}) \tag{2.1}$$

With $\boldsymbol{\xi}$, the vector of uncertain parameters, ψ_i the orthogonal functions and $\hat{u}_i$ the coefficients of those ψ_i functions. Uniform distributions use Legendre's polynomials whereas Gaussian distributions used Hermite's polynomials.

Knowing the number of needed evaluated point, a classical regression method is used to evaluate the coefficient $\hat{u}_i$. The following linear system to solve is then established [8]:

$$\begin{bmatrix} \psi_0(\boldsymbol{\xi}^1) & \psi_1(\boldsymbol{\xi}^1) & \cdots & \psi_P(\boldsymbol{\xi}^1) \\ \psi_0(\boldsymbol{\xi}^2) & \psi_1(\boldsymbol{\xi}^2) & \cdots & \psi_P(\boldsymbol{\xi}^2) \\ \vdots & \vdots & \ddots & \vdots \\ \psi_0(\boldsymbol{\xi}^n) & \psi_1(\boldsymbol{\xi}^n) & \cdots & \psi_P(\boldsymbol{\xi}^n) \end{bmatrix} \begin{bmatrix} \hat{u}_0 \\ \hat{u}_1 \\ \vdots \\ \hat{u}_P \end{bmatrix} = \begin{bmatrix} Y_1 \\ Y_2 \\ \vdots \\ Y_n \end{bmatrix} \tag{2.2}$$

With $P+1$, the number of terms in the truncated serie. The complexity of the regression solver rises dramatically with the number p of parameters and is also determined by the order of the orthogonal functions ψ_i. To meet accurate results, many evaluations have to be considered. The total number of evaluated points P is given by [7]:

$$P + 1 = \frac{(p+d)!}{p!d!} \tag{2.3}$$

With the amount of uncertain parameters p and d, the order of the orthogonal functions.

One additional strength of PCE is that the mean μ and the standard deviation σ of the investigated objective can be found easily thanks to the coefficients. For the purpose of reducing LCOX's mean and variance, this represents a computational asset.

$$\mu = \mu_0 \tag{2.4}$$

$$\sigma = \sqrt{\sum_{i=1}^{P} u_i^2} \tag{2.5}$$

2.2.4 Importance of uncertainties: Sobol indices

From the surrogate model established, it is possible to determine which uncertainty has high or minor impact on stochastic results. It is expressed through Sobol indices, from 0 to 1.

To determine if an uncertain parameters has much impact on the uncertainty of the outputs, *rule of thumb* is applied. If its Sobol indice is higher than the inverse of the number of studied parameters. In other words, if $Sobol(\xi_i) > \frac{1}{\#parameters}$, the uncertainty on the parameter is considered impactful on stochastic output.

2.2.5 RDO results

Robust optimizer

Robust design optimization is managed through two distinct loops, communicating with each other. The process is schematised here under (figure 2.2). One loop is responsible of the observation of uncertainties'impact for given design variables (**uncertainty loop**). Into the other one, a NSGA-II optimizer adapts the design variables that are put inside the uncertainty loop (**optimization loop**). The objectives of the optimizer are both minimizing the LCOX's mean and variance. An overview of NSGA-II solver algorithm is provided in appendices.

Uncertainty loop

For given design variables, a surrogate model of the energy system in developed via PCE-method. The inputs of this loop are:

- Parameters of the energy system (e.g., solar irradiance, heat and electricity demands)
- Mean, variance and distribution of uncertain parameters.
- Design variables from the optimizer (e.g., solar panels peak power, battery capacity, subsystem nominal power)

The output of the loop is a stochastic representation of the potential LCOX (Levelized Cost Of eXergy) for the given desgin variables and covering wide uncertainty possibilities through PCE-method.

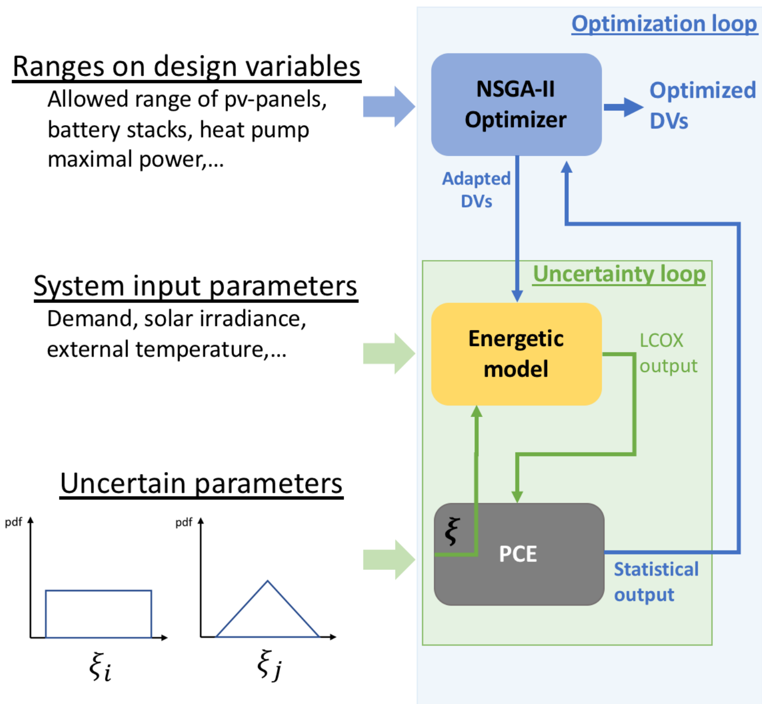

Figure 2.2: RDO uncertainty and optimization loops: the uncertainty loops manage the stochastic impact of the uncertain parameters on the model while the optimization loop's goal is to find the best set of design variables.

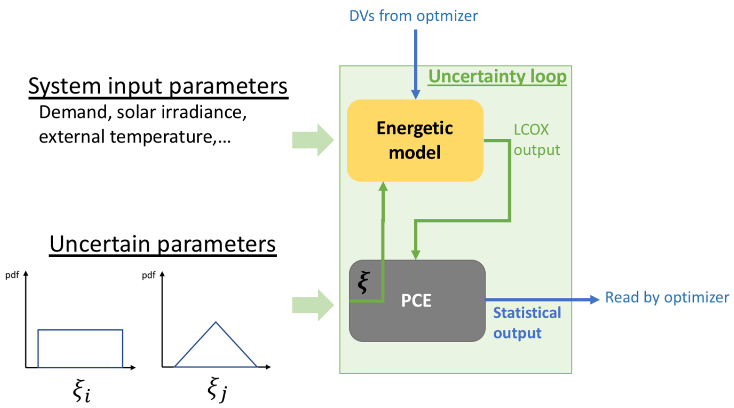

Figure 2.3: Uncertainty loop: for given design variables (DVs), the stochastic output of the model is evaluated. This step is done with the help of a surrogate model, build within the loop by PCE method.

Optimization loop

It modifies the design variables values given to the uncertainty loop through an optimizer. The inputs of this loop are:

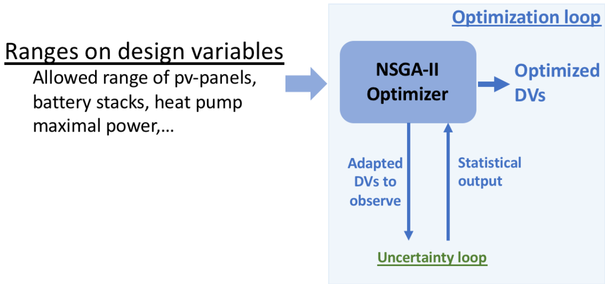

Figure 2.4: *Optimization loop*: the various possibilities of optimal design variables is investigated by the NSGA-II optimizer. It adapts the DVs in function of the uncertainty loop outputs to progressively establishing the best sets of DVs.

- Ranges for the decision variables values. It enables lower and upper limits for both exploring the field of possibilities and fix realistic limitations for the installations (e.g., a single rooftop can not hold 50[kWe] of solar panels).
- The stochastic results of the previous set of decision variables, provided by uncertainty loop.

As NSGA-II solver is based on a population evolution, multiple uncertainty loops are run to analyse a set of results that may lead to a optimized generation. The population is proportional to the amount of design variables (10 samples per design variables).

Representation of results

The evolving population of the NSGA-II optimizer creates a trade-off between the objectives, illustrated through non-dominated Pareto results. In the following figure2.5, a 10-individuals population has been dressed. For each individuals, there are no other configuration where an objective function can be improved without worsening the other (=*non-dominated sorting*).

The next figure (2.6) illustrates the expected results in the case of robust optimization. The two extremes cases (*lower mean design* and *robust design*) can be spotted, their design variables are thus retrieved and robustness of the system can be interpreted.

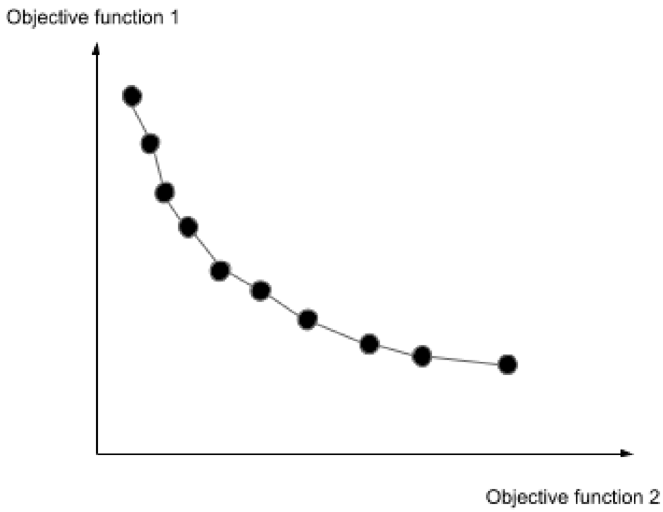

Figure 2.5: Representation of a Pareto front for a non-dominated sorted population of 10 individuals. The fictive dotted line follows the non-dominating sorting trend where no individual can enhance an objective without worsening the other.

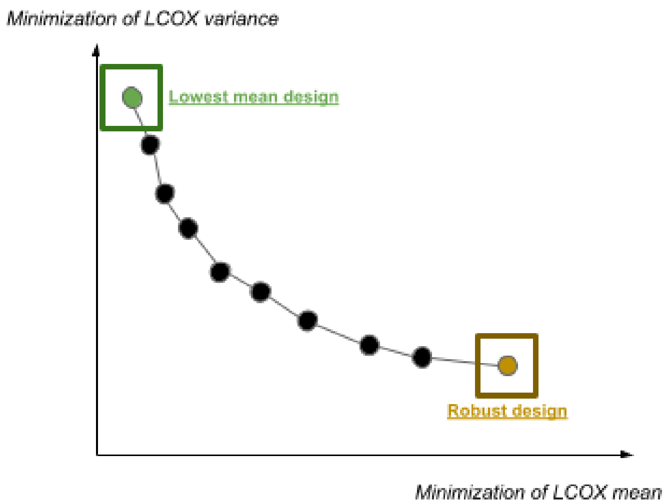

Figure 2.6: Trade-off between mean or variance minimization: the two extreme individuals are both maximizing one objective when minimizing the other. Those cases illustrates the trade-off between having precise idea around an expensive design (robust design) or minimizing the average probabilistic cost and worsening the precision on it (lower mean design).

Chapter 3

Modelling of the energy system

3.1 Shape of the studied system

The energetic system under investigation, see Figure 3.1, is composed of renewable and conventional energy sources. It shall not be purely self-sufficient and thus can exchange energy with the grid network and city gas to cover both electric and heat demands.

The photovoltaic array and battery stack are connected via a DC-DC converter to a DC busbar. A DC-AC inverter connects the DC busbar to the load. When the PV array matches the demand, the excess of electricity is used to charge the battery and the excess of electricity is sold to the grid.
Otherwise when the PV electricity fails to comply the demand, the battery stacks are discharged and additional support can be provided by the grid when the SOC (State Of Charge) is at its lowest limit (20%) .
The gas boiler is used to cover the heat demand. In the whole study, no distinctions are made between space heating and dwelling heating water.

3.1.1 Photovoltaic array

A photovoltaic array is characterized by the single diode model of PVlib Python library [9]:

$$I_{PV} = I_L - I_0\left(\exp\left(\frac{U + IR_s}{n_{diode}N_sU_{th}}\right) - 1\right) - \frac{U + IR_s}{R_{sh}} \tag{3.1}$$

The parameters of the Equation 3.1 are determined thanks to the method developed by De Soto et al. [10]. The resulting current-voltage characteristic provides the power output in function of the solar irradiance and ambient temperature. As the PV array is connected to a DC-DC converter with Maximum Power Point Tracking, the maximum power point is always assumed to be reached.

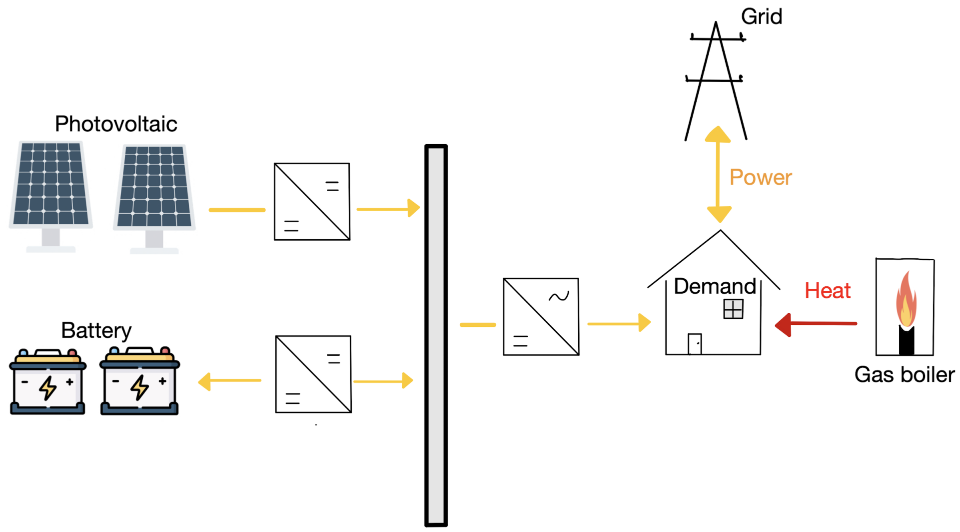

Figure 3.1: Basic system shape.
The photovoltaic-battery-gasBoiler system consists of photovoltaic array that primarily complies with the electricity demand. If it is not sufficient, the grid is used as a back-up power generator. When there is an excess of electrical power produced, the battery stacks are charged and the system sells the excess of electricity to the grid. Heating demand is covered by gas boiler and no distinction are made between space heating and dwelling heating water.

3.1.2 Battery stack

The lead-acid battery technology [11] is used to simulate the electric storage. The model of Blaifi et al.[12] characterises the battery stack and the voltage-current relation is defined as:

$$U_{bat} = U_{bat,oc} + I_{bat}R_{bat} \tag{3.2}$$

$U_{bat,oc}$ is the open-circuit voltage, R_{bat} is the resistance component which determines the voltage evolution after charging and discharging. R_{bat} is temperature sensitive and depends also on current magnitude and capacity [12]. The battery current I_{bat} is positive during charge and negative during discharge.

The SOC represents the amount of electricity stored in the battery:

$$SOC(t) = SOC_0 + \frac{1}{C(t)} \int_0^t n_{bat}(t)I(t)dt \tag{3.3}$$

In Equation 3.3, SOC_0 is equal to 20% [13, 14]. The SOC significantly affects the battery lifetime, which is determined through the Rainflow cycles counting method [15]. The lifetime is impacted by the use of the battery, thus overcharging and discharging are avoided. The maximum charging current and maximum discharging current are limited to avoid an excessive reduction of the battery lifetime [16].

3.1.3 Power converters

The battery stacks and PV array are connected to a DC busbar through DC-DC converters [17]. A DC-AC inverter connects the DC busbar to the load to fulfill the demand and allows to sell the excess of electricity to the grid. The efficiency of DC-DC and DC-AC are fixed [18, 19].

$$P_{DC,out} = 0.90 P_{DC,in} \tag{3.4}$$

$$P_{AC,out} = 0.95 P_{DC,in} \tag{3.5}$$

3.1.4 Gas boiler

The gas boiler covers the heating demand of the dwelling. In this study there is no distinction between space heating and dwelling heating water. It produces heat with a nominal efficiency of 0.9 [20].

3.2 Climate and demand data

On Figure 3.2, the hourly climate and demand data are presented. The system is evaluated in Brussels over one year. The data exploited is a Typical Meteorological Year provided by the National Renewable Energy Laboratory [21, 22]. As the data are related to United States, the method presented by Montero Carrero et al.[23] is used, to scale the heating demand and electrical demand profiles for Belgium.

3.3 Objective and design variables

The Levelized Cost Of eXergy (LCOX) takes into account the quality of different energy flux and allows us to compute the cost of a system composed by different type of energy [24]. This quantity of interest, the LCOX, reflects the system cost per unit of exergy covered [25]:

$$LCOX = \frac{CAPEX_a + OPEX_a + C_{r,a} + C_{e,a} + C_{g,a}}{X_{demand}} \tag{3.6}$$

In the Equation 3.6, the cost entities in numerator are annualized. It means that their financial impact are reported on a one year consumption, taking the life time of the system into account. $CAPEX_a$ and $OPEX_a$ are respectively the annualized investment cost and operational cost and $C_{r,a}$ is the annualized replacement cost and $C_{e,a}$ is related to the electricity bought from the grid while $C_{g,a}$ is the annualized gas cost. The quantification of these parameters comes from the paper of Zakeri et al. [25]. The annual exergy output X_{demand} is characterized by the sum of the annual exergy required for electricity and heat [26]:

$$\sum_{i=1}^{8760} \sum_{type} X^t ype, \qquad type \in \{elec, heat\} \tag{3.7}$$

whereas the electricity demand is covered by the highest energy quality, i.e. $X^{elec} = E^{elec}$, the Carnot Factor F [26] scales the exergy covering the heating demand:

$$X^{type} = F^{type} E^{type}, \qquad type = heat \tag{3.8}$$

$$F = 1 - \frac{T_{amb}}{T_{req}} \tag{3.9}$$

where T_{amb} corresponds to the ambient temperature for each specific hour of the year and T_{req} corresponds to the temperature required to fulfil the heating demand, set at $55°C$ for the heat produced by the gas boiler [27].

The design variables are the battery stack and PV array capacity, respectively n_{bat} and n_{pv} (in [kWh] and [kWp]).

3.4 Results

The robust design optimization results illustrate the trade-off between minimizing the mean and the standard deviation of the LCOX see Figure 3.3. Let's define two designs of interests:

- The **mean optimal design**: the point at the extreme left of the Pareto front, minimizing the mean μ_{LCOX} at most. It corresponds to the cheapest optimal design but the less reliable on prediction precision.
- The **robust optimal design**: the point at the extreme right of the Pareto front, minimizing the standard deviation σ_{LCOX} at most. It corresponds to the optimal design with the better stochastic accuracy on LCOX mean value. On the other hand, it is also the most expensive design as "beating uncertainties" involves larger investments (i.e., installing more PV-panels to enhance self-sufficiency and thus rely less on uncertain cost grid electricity).

As you can see on the Pareto front (Figure 3.3) the reduction of the LCOX standard deviation is relatively small (about 4 [€/MWh]) and it leads to an increase of the LCOX mean of 43 [€/MWh].

Explanation of this evolution: First, let's recall that the leverage of the optimizer is the adjustment of the two design variables, the photovoltaic capacity installed in [kWp] and the battery stack capacity in [kWh]. Then, the only way to achieve a robust optimal design is to play on those decision variables. A robust optimum is achieved by rising those installations as the system will be less dependent on the grid. As you can see in Table 3.1, the value of Sobol indices of parameters related to the grid electricity decreases and this is exactly what is expected when a larger PV-battery system is installed. However, larger deployment of costly technology leads to an increase of the LCOX mean value.

	Mean optimal design	Robust optimal design
gas_cost	0.72	0.77
elec_cost_ratio	0.12	0.05
boiler_eff	0.07	0.07
uq_load_e	0.04	0.06
uq_load_h	0.03	0.03
elec_cost	0.03	0.01

Table 3.1: Sobol indices of the most important parameters for the mean optimal design (on the left) and the robust optimal design (on the right).

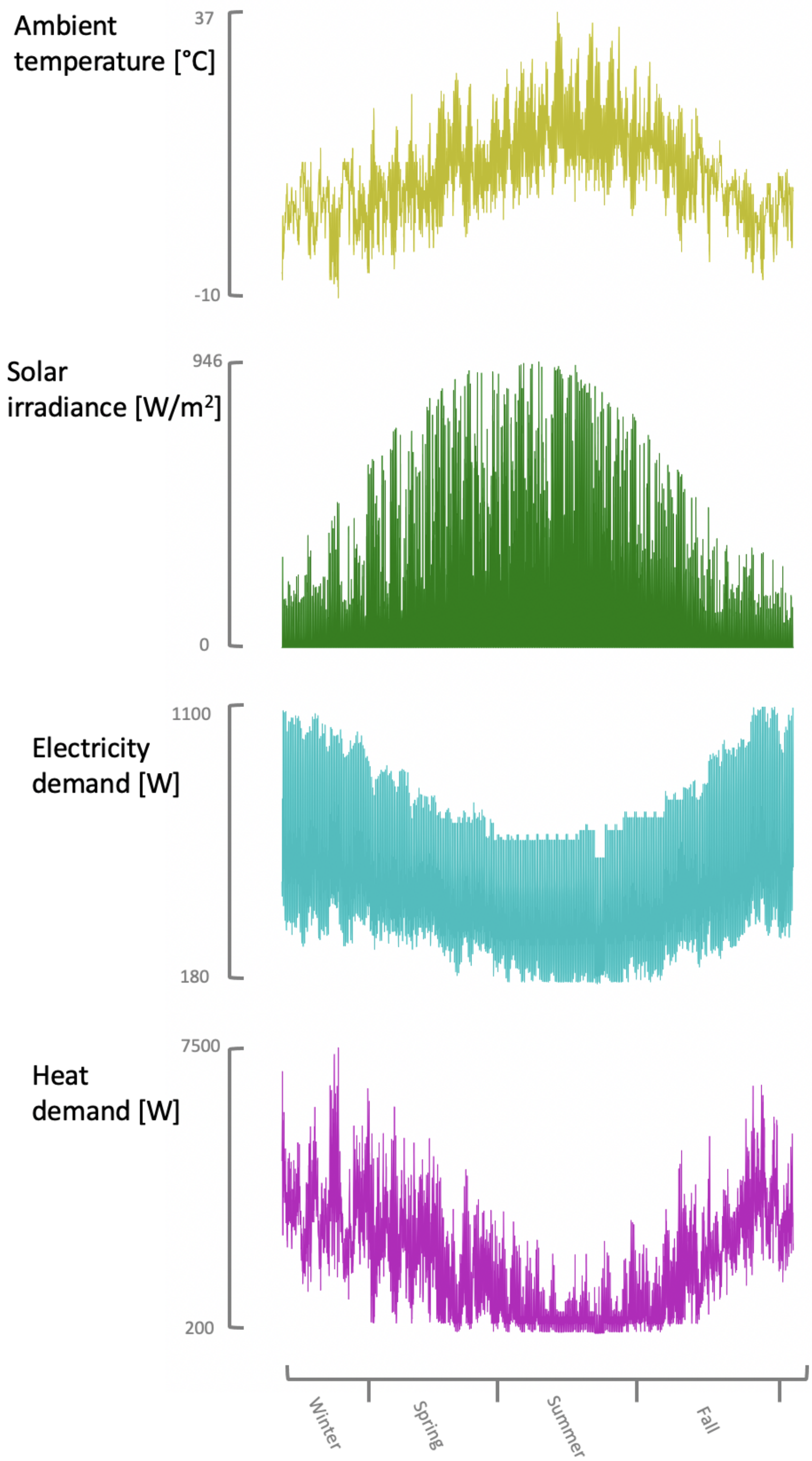

Figure 3.2: The hourly solar irradiance and ambient temperature are increasing during spring and summer, while declining during fall and winter. Consequently, the hourly electricity and heating demand data drop during spring and summer and increase during fall and winter.

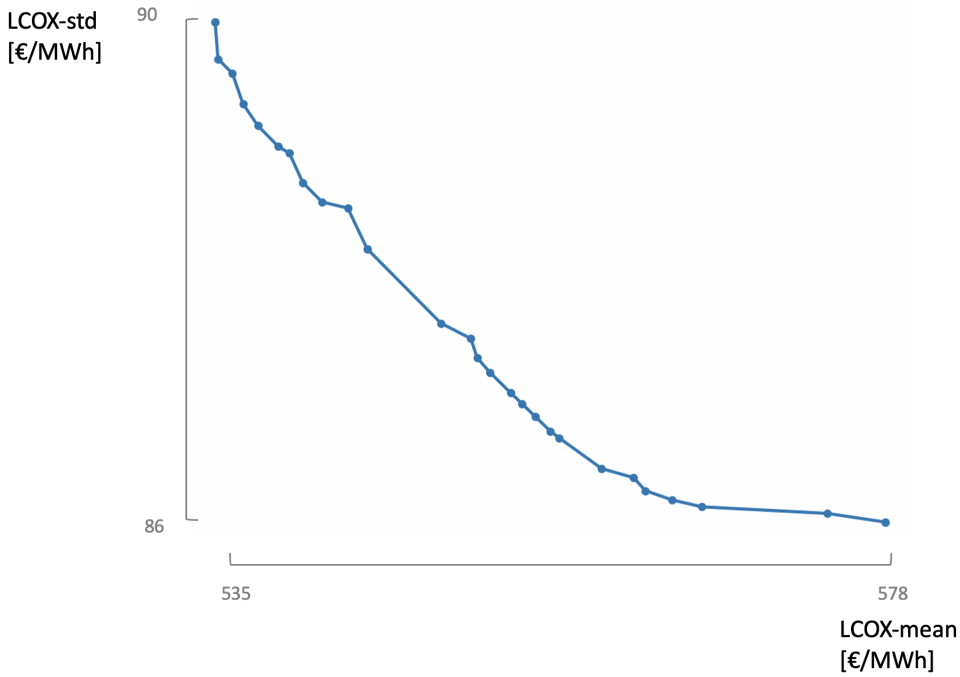

Figure 3.3: The Pareto front between minimizing the LCOX mean value and minimizing the LCOX standard deviation illustrates that the gain in robustness is limited when shifting between optimized mean value and robust design. The Sobol' indices explain this limited gain in robustness by illustrating that the aleatory uncertainty on the gas price (see Table 3.1), which is irreducible by designing the PV array and battery stack capacity, is the main driver of the LCOX standard deviation.

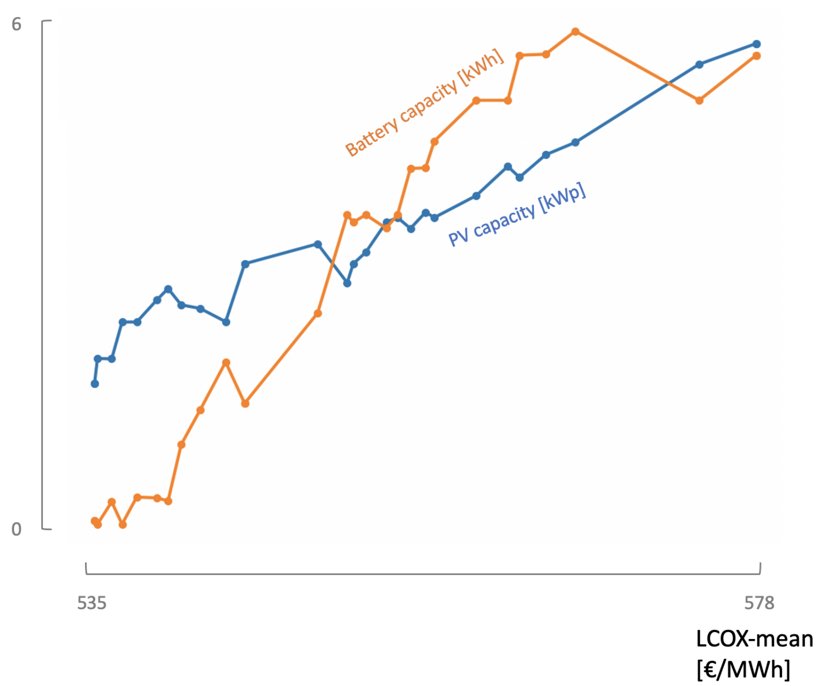

Figure 3.4: The design variables of the system are the photovoltaic capacity installed [kWp] and battery stack capacity [kWh]. To reduce the LCOX standard deviation, the optimizer will increase the PV and batteries capacities in order to reduce their dependence to the grid which is subject to uncertainties.

Chapter 4

Micro gas turbine connection

4.1 Theoritical recap

4.1.1 Basic gas turbine

A gas turbine utilizes the flow from hot gases produced from combustion of gas or fuel oil, to produce kinetic energy within a turbine. When a generator is connected to the gas turbine, the kinetic energy is converted to electricity. The basic gas turbine installation is composed by three main elements i.e. compressor, combustion chamber and turbine(see Figure 4.1).
Fresh air is drawn within a **compressor**, rising its pressure and temperature. The compressed air proceeds into the **combustion chamber**, where fuel is ignited. The high temperature resulting gases enter the **turbine**, where they expand themselves down to atmospheric pressure while making the turbine rotates. The kinetic energy from the rotation is recovered in electricity through the use of an electromechanical convertor.

The T-s diagram on Figure 4.1 shows an ideal gas cycle, also known as Brayton cycle. The Brayton cycle is made up of four internally reversible transformations [28]:

$1-2$ Isentropic adiabatic compression

$2-3$ Combustion at constant pressure

$3-4$ Isentropic adiabatic expansion

$4-1$ Heat rejection at constant pressure

To enhance the global efficiency of the installation, a **recuperating cycle** can be implemented. The idea is to utilize back the hot exhaust gases to preheat the air entering the combustion chamber. The heat recycling is done by a recuperator, working as a counter flow heat exchanger, as shown in Figure 4.2. By preheating the

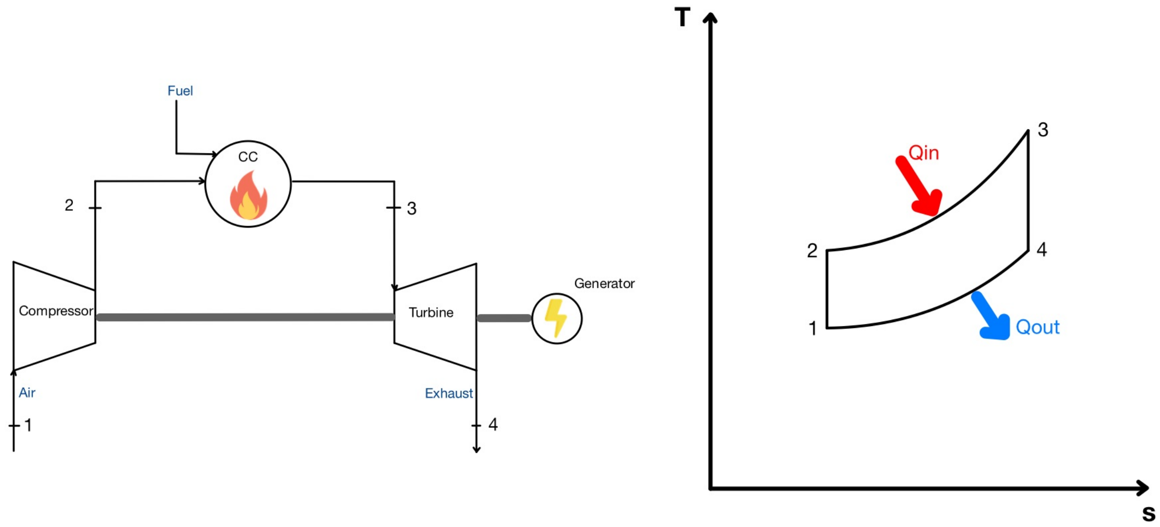

Figure 4.1: Gas turbine schematic (left) and the Brayton cycle (right).
Air enters at ambient pressure and temperature and is compressed to a certain pressure p_2. Between stages 2 and 3, gas is injected and combustion takes place, the flue gases reach a certain Turbine Inlet Temperature (TIT). At the level of the turbine, the useful work is produced by the expansion of the gases along its blades.
The compression and expansion are assumed isentropic and heat exchanges are isobare.

compressed air, lesser heat has to be produced in the combustion chamber, resulting in less fuel consumption. Those savings lead to an efficiency improvement of the basic installation.

Moreover, after the recuperator, an economizer can retrieve residual heat from the exhaust gas flux to warm up water, beneficial for both domestic hot water or space heating.

4.1.2 Micro gas turbines

The micro gas turbines (MGT) are small scale gas turbines that produce power approximately from 10–200 [kW]. In comparison, regular gas turbines are engines ranged in [MegaWatts][29]. The MGTs are characterized by their simplicity, their flexibility and their affordability. Those characteristic make them excellent candidates for providing base load and cogeneration power for small scale demands. Microturbines usually come as a combined heat and power (CHP) system. The unit produces electricity (as mentioned in the previous section) and utilizes the exhaust heat from the turbine to heat up water.

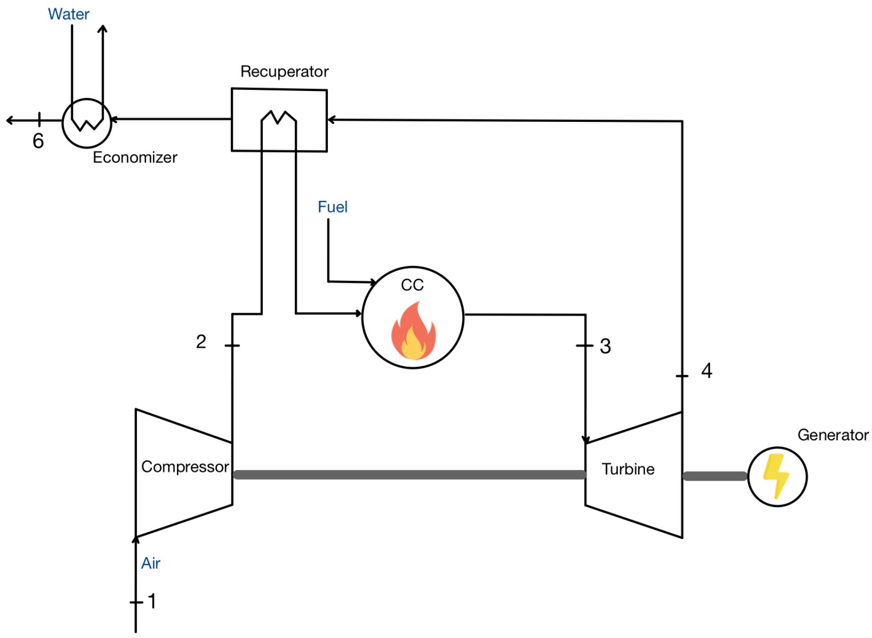

Figure 4.2: A heat recuperator is added to the standard GT scheme. It preheats the air before entering the combustion chamber and therefore reduce the exegetic losses at the combustion chamber. The remaining heat at the output of the recuperator enters in an economizer to heat the water circuit.

4.2 MGT unit and characteristics

The **Turbec T100** unit is the MGT inserted in the study. It produces at nominal conditions $100[kW_{elec}]$ and $165[kW_{th}]$ with an electrical efficiency of $\eta_{elec} \approx 0.30$ and a global energetic efficiency $\eta_{tot} \approx 0.8$. The main components of the unit include a gas turbine engine, an electrical generator, an exhaust gas heat exchanger and control systems. The gas turbine engine operates on a single shaft (i.e. the compressor is mounted on the same shaft as the turbine and generator, as shown in Figure 4.2). Ambient air is drawn into the unit and compressed by a centrifugal compressor. The pressure ratio for this system is about 4.5: 1. Compressed air leaving the compressor enters the recuperator, as illustrated in Figure 4.2. Afterwards, the preheated compressed air is mixed with natural gas and ignited, leading to an increase in energy flux. The resulting combustion gases flux enters the turbine with a high energetic content (high pressure and temperature around 950 °C). It expands itself within the turbine and before leaving it with a pressure close to atmospheric pressure and a temperature of approximately 650 °C. A permanent rotating magnet in the generator generates the electric power. The generated electric power needs to be rectified and transformed to preferred frequency before entering the grid [30].
After the expansion in the turbine the exhaust gases enter the recuperator before

entering the gas-water counter-current heat exchanger with a temperature of approximately 270 °C. By regulating the mass flow of the water, the water is heated up to a desired temperature.
Furthemore, an automatic control system, PMC (Power Module Controller), supervises and controls the Turbec T100 behavior. This prevents the system from critcal distortion by shutting it down by itself.

4.3 Modelling of the system

The energetic system investigated follows the exact same scheme as the one introduced in Section 3.1, except that a micro gas turbine unit is added, see Figure 4.3.
Reminder: the photovoltaic array and battery stack are connected via a DC-DC converter to a DC bus bar. A DC-AC inverter connects the DC bus bar to the load. When the PV array match the demand, the excess of electricity is used to charge the battery and excess of electricity is sold to the grid.
Otherwise when the PV electricity fails to comply the demand, the battery is discharged and then the demand is supported by the grid **or the CHP unit**.

4.3.1 Filling the heat demand

The micro gas turbine is used to fulfill the heating demand and when it is not sufficient, gas boilers are started to comply with the remaining heat. If the demand is lower than half of the nominal power of the CHP ($\frac{165kW_{th}}{2}$), the unit is in standby and gas boilers respond to the demand. In this study they are no distinctions between space heating and domestic hot water.

4.3.2 Efficiencies and lifetime

As said in the previous section, the Turbec T100 nominal characteristics are 100 $[kW_{elec}]$ and 165 $[kW_{thermal}]$. The electrical efficiency is $\eta_{elec} \approx 0.30$ and it has a thermal efficiency close to 50% [31]. The part load electrical efficiencies and thermal power output are depicted in Figure 4.4.

Ambient conditions such as temperature, affect the performance of CHP units as the electrical efficiency is getting worse with rising inlet air temperature. For example, for the case of the T100 MGT, the electrical efficiency descends from 30% at 15 °C to 29.4% at 20 °C [31]. However, this phenomenon is not taken into account in this study, considering that it would not impact the model results.
In the model, the MGT has a lifetime of 60.000 hours of operation [31]. Above this

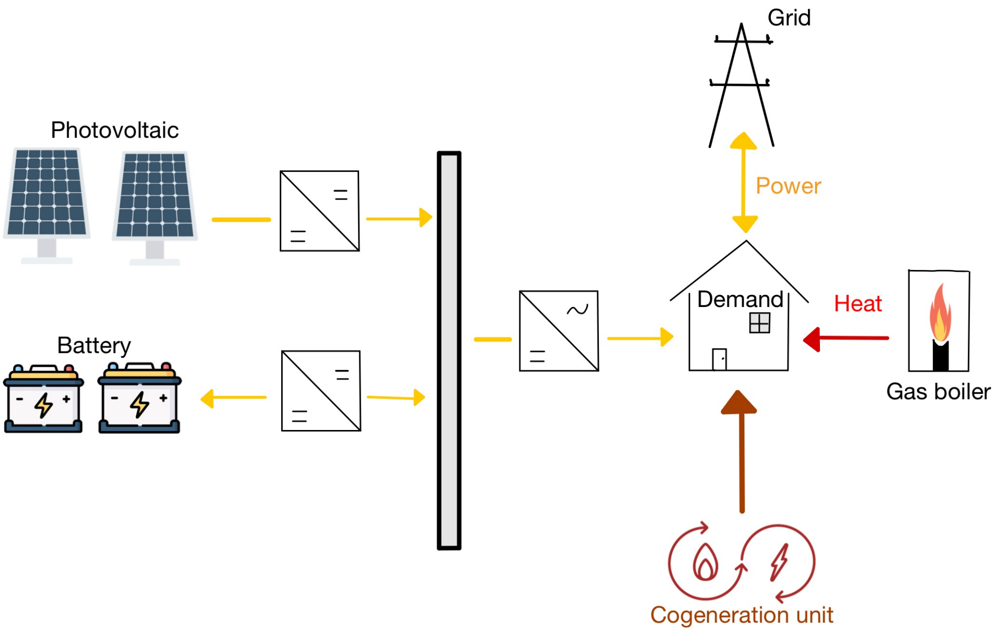

Figure 4.3: The photovoltaic-battery-boiler-MGT system consists in a PV field that primarily complies with the electricity demand. The grid is used as a back-up power generator when the MGT is not sufficient enough. When there is an excess of electrical power produced, the battery are charged and the system can sell to the grid the excess of electricity. Heating demand is covered by MGT and no distinction are made between space heating and dwelling heating water. When the heating demand is out of the range of utilization of the CHP unit, gas boilers are used.

threshold, dramatic increase in Operation & Maintenance (O&M) costs are expected.

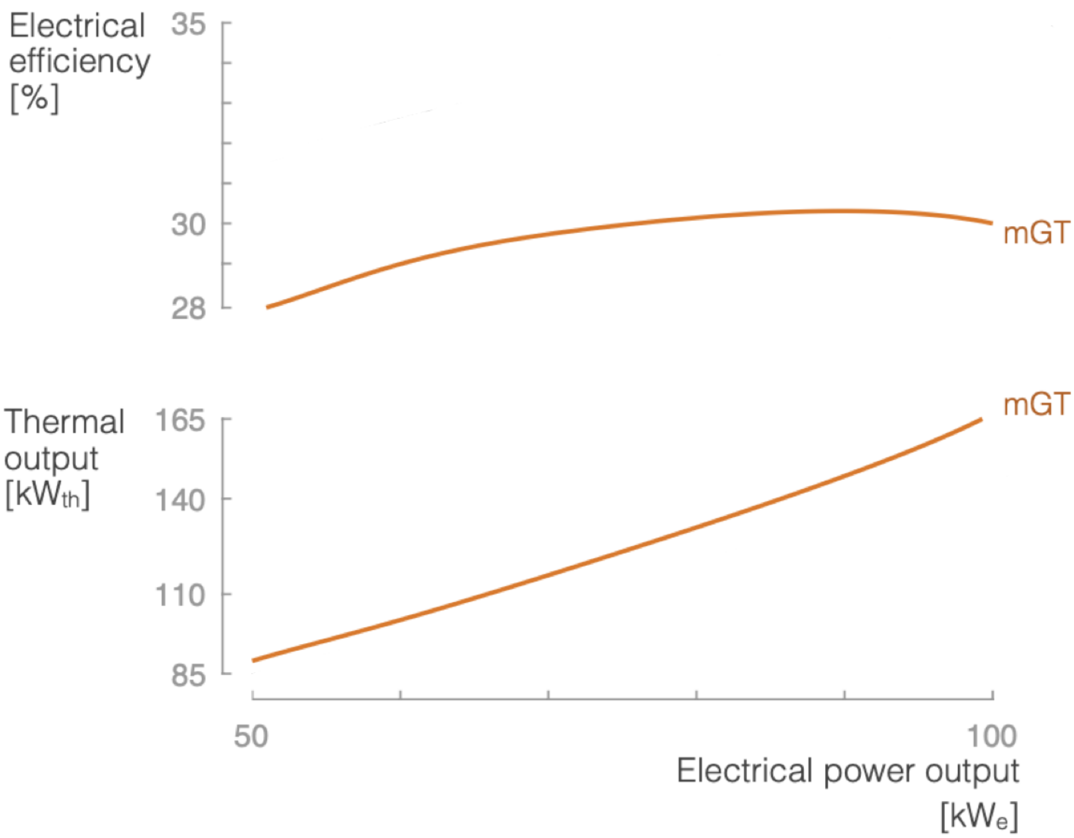

Figure 4.4: The MGT offers an electrical efficiency ranging from 28% to 30%. The cycle presents a thermal efficiency ≈ 50%. Data source: [31].

4.4 Uncertain parameters

The Table 4.1 shows all the parameters related to the MGT unit. Those are added to the basic model ones related in Section 3.1. In this section, you will have a quick justification of where do they come from.
The standard deviation σ of each parameter correspond to 5% of the mean value μ .

4.4.1 Investment and maintenance

The installation costs of the CHP unit:
Due to the lack of informations, no distinctions have been made between the installation cost of ICE and MGT. These include a variety of issues. Based on real

	Unit	Distribution	μ	σ	Range
$CAPEX_{MGT}$	€$/kW_{th}$	Uniform	2600	130	$[2470; 2730]$
$OPEX_{MGT}$	€$/kWh_{th}$	Uniform	0.015	0.00075	$[0, 01425; 0, 01575]$
Unit lifetime	$Hours$	Uniform	60 000	3000	$[57.000; 63.000]$
Replacement costs	€$/kW_{th}$	Uniform	2100	105	$[1995; 2205]$

Table 4.1: Uncertain parameters of the MGT unit.

cogeneration ICE machines currently operating in Brussels, these costs were estimated equal to 80 000 € for MGT unit [32].
O&M costs:
This value comes directly from this paper [33]. It reflects all the expenses linked to the use and maintenance of the MGT.

4.4.2 Lifetime of the unit

The lifetime (in years) of each technology depends on the running hours of the unit. For the MGT unit, it turns around 60 000 running hours, after that it would be replaced because the O&M costs soar. [31].

4.4.3 Replacement costs

No information have been found what concerns replacement costs of the cogeneration unit. They thus have defined a bit lower than the CAPEX, see Table 4.1.

4.5 Quantity of interest and design variables

The design variables are the battery stacks capacity, the total PV-array peak power and the number of load, respectively n_{bat}, n_{pv} and n_{load} (in [kWh], [kWp] and [number of dwellings]). The use of this "number of loads" design variable is justified by the fact that the range of power produced is much more higher than a single load dwelling ($< P_e > \simeq 500[W_e]$, $< P_h > \simeq 2[kW_{th}]$). The quantity of interest is still the Levelized Cost Of eXergy (LCOX), as presented in Chapter 3.

4.6 Results discussion

4.6.1 Scenario 1: not selling electricity, MGT-GasBoilers

The current investigated scenario do not allow the selling of excess of electricity to the grid. The robust design optimization results illustrate the trade-off between minimizing the mean and minimizing the standard deviation of the LCOX, see Figure 4.5. The lowest mean (880.78 [€/MWh]) is achieved by a total of 37.5 [kWp] of PV arrays, 2 [kWh] of battery and a number 16 dwellings. Reducing the LCOX standard deviation is then achieved by increasing the PV array capacity, followed by the inclusion of a battery stack and the reduction of the demand thanks to the number of dwellings design variable, Figure 4.6. This increase of technology installed reduces the dependency on the electricity price uncertainty.

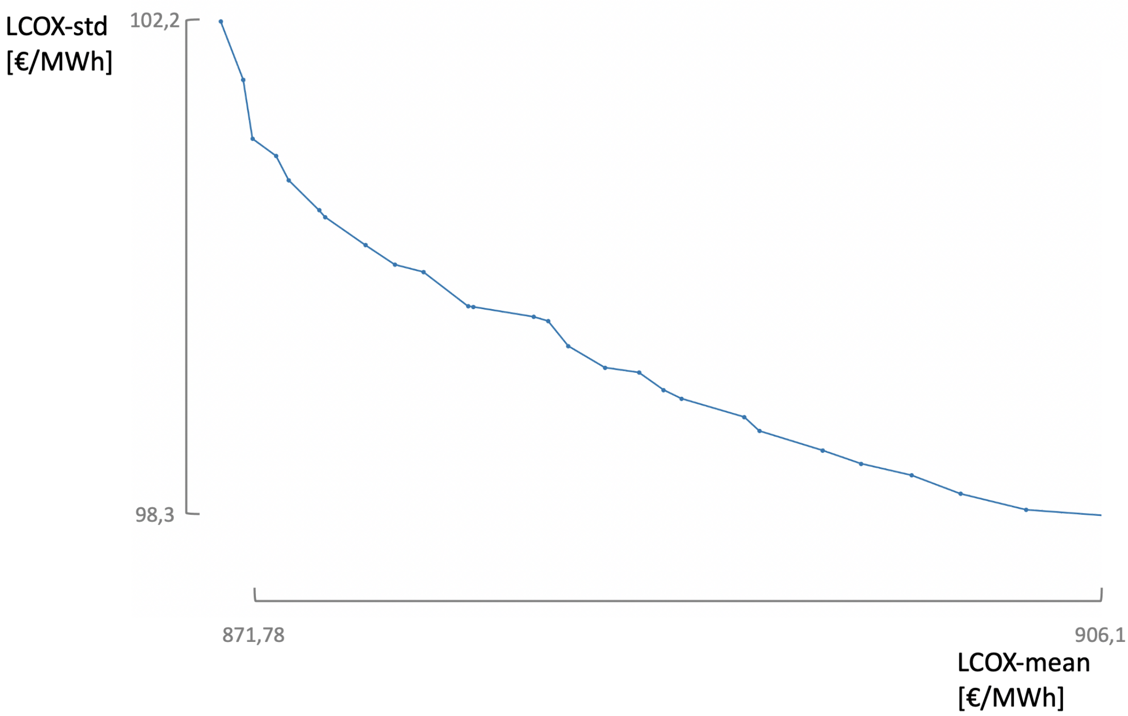

Figure 4.5: In this 1st scenario, the Pareto front illustrates that a trade-off exists between minimizing the LCOX standard deviation and the LCOX mean. The PV capacity and the number of dwellings are quite constant, on the other hand there is an increase of the battery capacity installed.

The heat is 100% provided by a gas consumption whose price is subject to a certain uncertainty. So the only way to reduce the impact of this parameter is to reduce the consumption of gas. This is handled by the n_{load} design variable, see Table 4.2. As you can see in Figures 4.7a and 4.7b, it is not sufficient because the gas price's

Sobol index stay constant between the mean optimal and robust optimal designs. As the PV-battery system only affect the amount of grid electricity consumed, its deployment has little effect on LCOX uncertainty.

	n_{PV} [kWp]	n_{bat} [kWh]	n_{load} [-]	μ_{LCOX}	σ_{LCOX}
mean optimal design	37.5	2	16	880.78	102.2
robust optimal design	46.5	76	12	906.1	98.3

Table 4.2: Characteristics of the mean optimal design and the robust optimal design

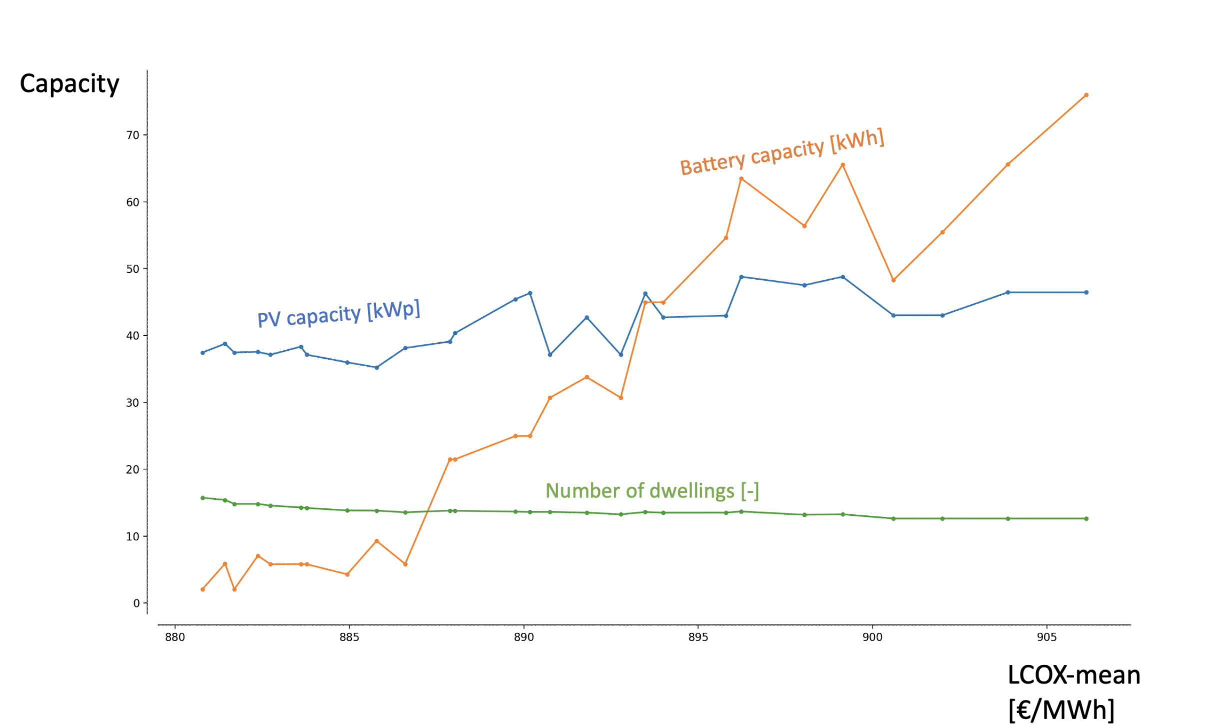

Figure 4.6: Evolution of the design variables when minimizing the LCOX's mean and standard deviation, in the PV-BAT-MGT-GasBoilers energy system. The PV capacity and the number of dwellings are quite constant, in the other hand there is an increase of the Battery capacity installed.

The Sobol' indices represented in Figures 4.7a and 4.7b clearly illustrate that the variation of the LCOX standard deviation is mainly due to the uncertainty on the gas price, the electricity load and the electricity cost ratio. This last parameter illustrates the part of the electricity price that corresponds to the cost of the electrical energy. For example in Brussels, approximately 30% of the electricity bill is related to the TSO (Transmission system Operator) costs.

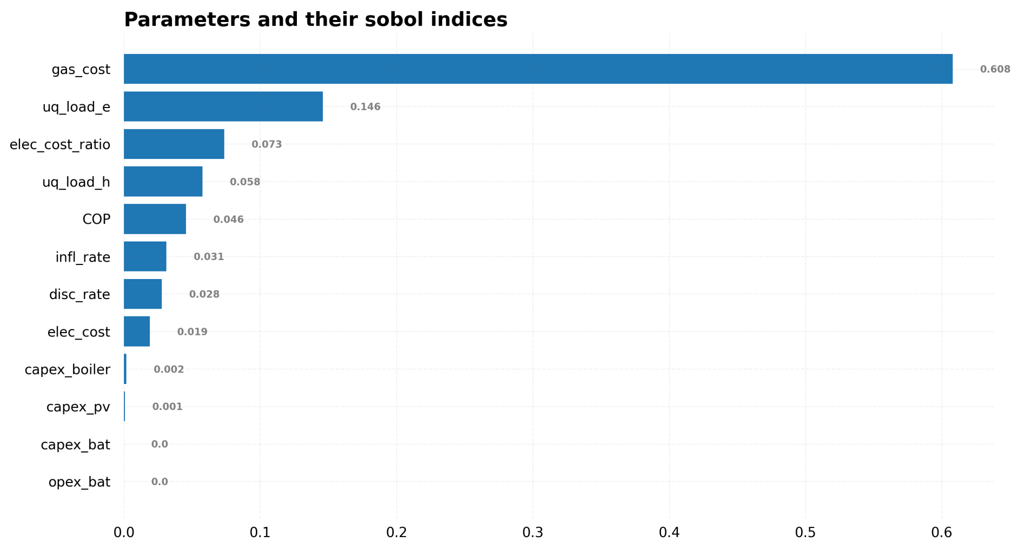

(a) Sobol indices **mean optimal design**

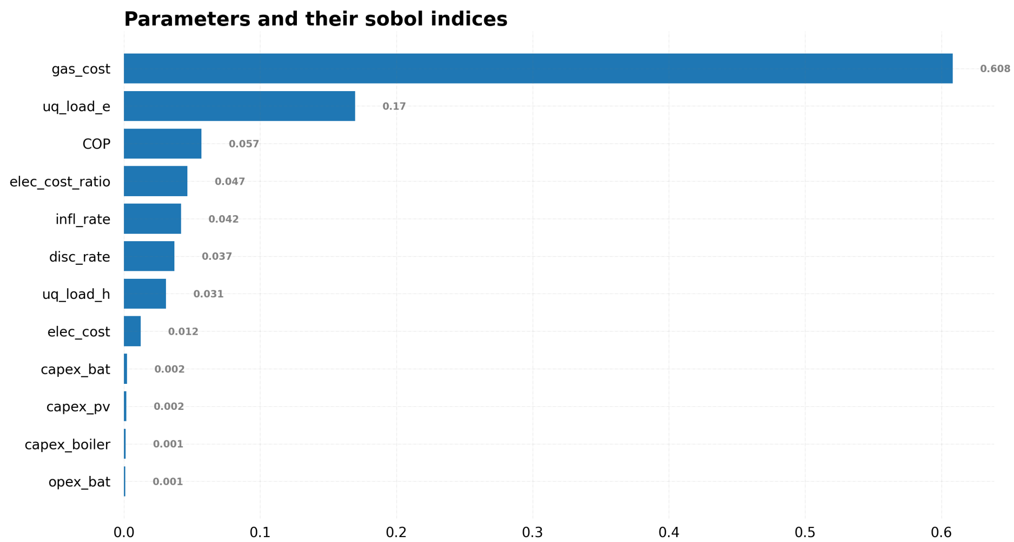

(b) Sobol indices **robust optimal design**

Figure 4.7: Sobol indices of the main parameters of the PV-BAT-MGT-GasBoiler energy system. Two designs are presented here, the mean optimal design (a) and the robust optimal design (b).

Another observation is that by reducing the n_{load} design variable to the values presented in the Table 4.2, the use of the MGT is limited. As a reminder, the MGT's power management is driven by the heat demand, and the heat demand is directly

proportional to the number of dwellings (n_{load}). In order to reduce the uncertainty coming from the price of the gas, the optimizer encourages the use of the gas boiler and shut down the cogeneration unit as much as possible. In this configuration the MGT covers only 2% of the heat demand.
Therefore to take advantage of the installed technology, let's change the gas boiler by an electrical boiler.

4.6.2 Scenario 2: not selling electricity, MGT-ElecBoiler

When the gas boiler is replaced by electrical boiler, the robust design optimization shifts the Pareto front (of the previous case) to the left and the LCOX's standard deviation rises (LCOX-std), see Figure 4.8. This strategy has an impact on the standard deviation of the LCOX, there is an increase of $\approx 13\%$ in the robust optimal design. For the lower mean design, a negative 10% difference can be observed between current scenario and previous one, using gas boilers, Table 4.4.

	$\boldsymbol{\mu_{LCOX}}$ **range**	$\boldsymbol{\sigma_{LCOX}}$ **range**	$\boldsymbol{n_{load}}$ **range**
Scenario 1: gas boilers	[881-906]	[98-102]	[12-16]
Current scenario	[796-884]	[114-121]	[42-59]

Table 4.3: Comparison between previous scenario and current scenario (gas boilers vs. electric boilers as secondary heat source).

	n_{PV} [kWp]	n_{bat} [kWh]	n_{load} [-]	μ_{LCOX}	σ_{LCOX}
Mean optimal design	58.2	0.70	58.7	795.82	121,35
Robust optimal design	119.77	251.11	42	883.85	114.08

Table 4.4: Characteristics of the **mean optimal design** and the **robust optimal design** when gas boiler is replaced by electrical boiler.

As presented in Table 4.4, the range of the LCOX mean is lower than in the previous case, it evolves from 795.82 to 883.85 [€/MWh]. This shift to the left could be explained by the fact that the number of dwelling is higher [58.7 ... 42] (see Figure 4.9), and as heat demand increases with n_{load}, the more often the MGT goes into action. When the cogeneration unit is running, it produces heat and electricity and this is why a decrease of the LCOX mean's range is observed.

The standard deviation of the LCOX is higher, the range goes from 121.35 to 114.08 [€/MWh] as shown in Figure 4.8.
In this scenario, the electrical boiler takes the place of the gas boiler. The electricity that feeds the boiler is subject to two uncertain parameters, the cost of electricity

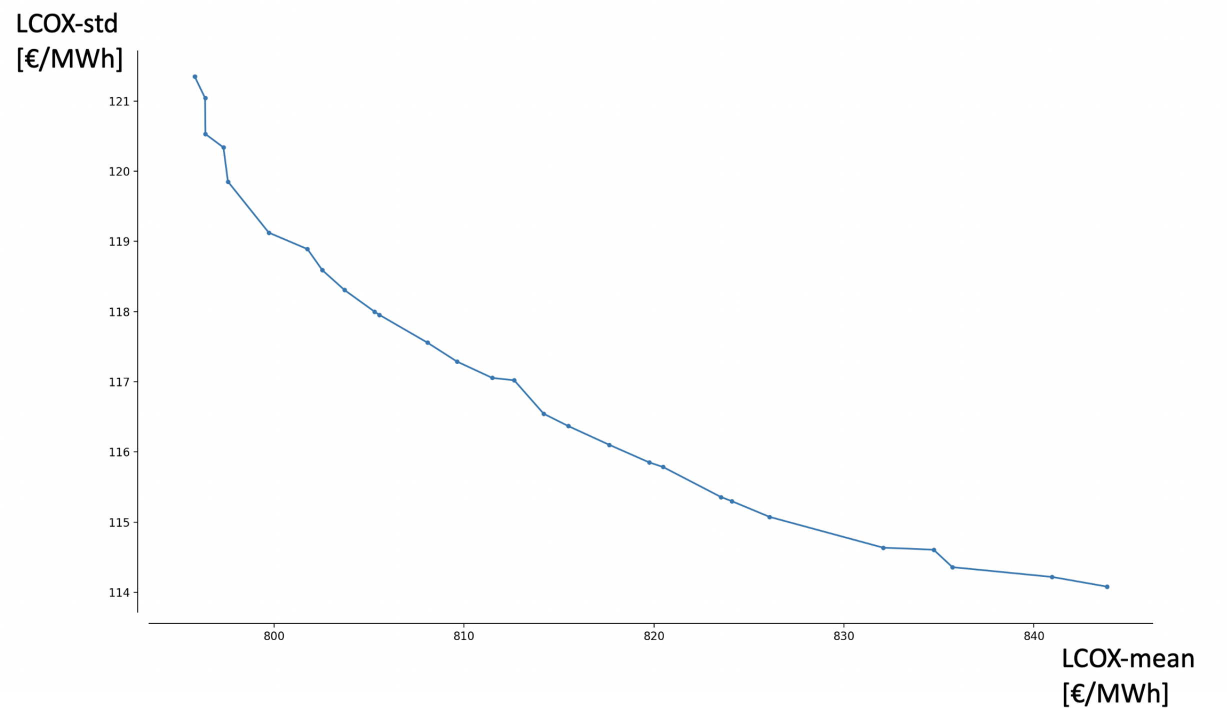

Figure 4.8: The Pareto front illustrates that a trade-off exists between minimizing the LCOX standard deviation and the LCOX mean. To pass from the mean optimal design to the robust optimal design, the optimizer doubles the PV capacity installed and avoid grid dependency by including batteries. The number of dwellings is reduced from 49.26 to 35.15.

(elec_cost) and the part of electricity bill that really corresponds to the electrical energy (elec_cost_ratio). In the previous case, the only part of uncertainty of the gas boiler was coming from the price of the gas (gas_cost). This should be the reason of the increase of LCOX-std.
Now let's investigate in the evolution of the Pareto front of electrical boiler scenario.

In order to decrease the uncertainty on the LCOX, the optimizer doubles the PV capacity, includes more batteries (251.11 [kWh]) and reduces the number of dwellings, see Figure 4.9 and Table 4.4.
First of all, the inclusion of the batteries and the increase of the PV capacity reduces the Sobol indices related to the electricity (elec_cos_ratio and elec_cost). As you can see in Table 4.5, the reduction of the number of households also reduce these uncertainties because it reduces the purchase grid electricity.
Secondly, let's focus on 25% increase of gas_cost Sobol index. At first sight it may seem strange because the number of dwellings decreases in the robust design. For this reason it is interesting to look at the SSR_{heat} in Table 4.5, this value reflects

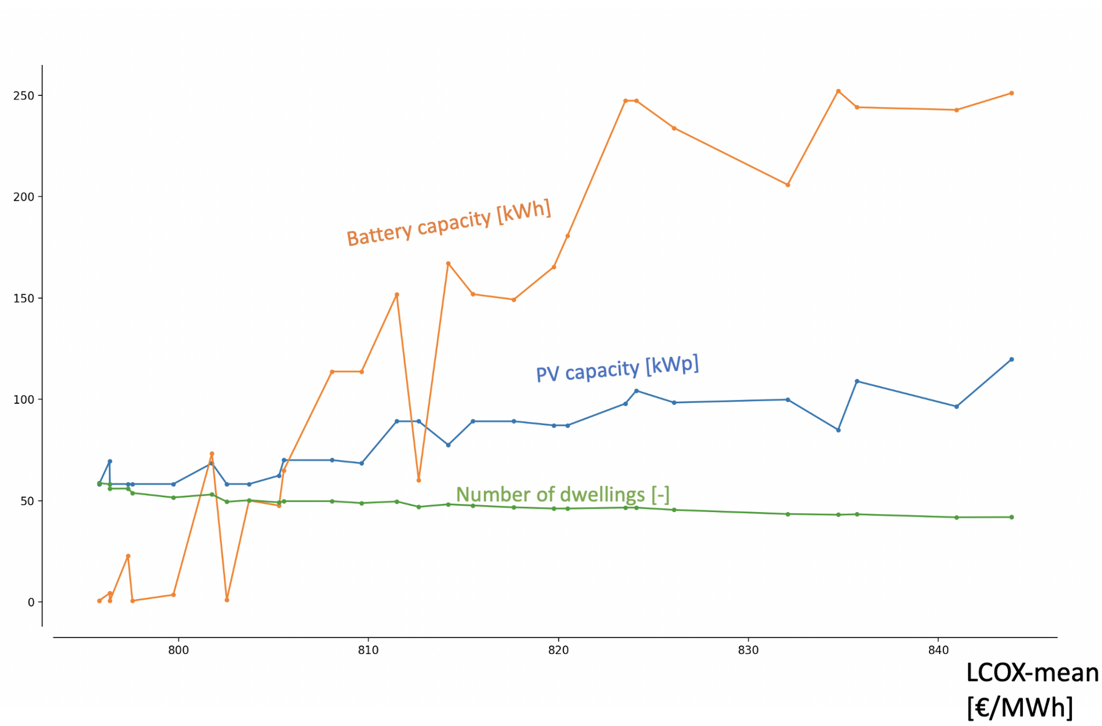

Figure 4.9: Evolution of the design variables when minimizing the LCOX mean and standard deviation, in the PV-BAT-MGT-ElecBoilers energy system. The PV capacity and the number of dwellings are quite constant, in the other hand there is an increase of the Battery capacity installed.

	mean optimal design	robust optimal design	units
μ_{LCOX}	795.82	883.85	$€/MWh$
Elec load	257.21	183.49	MWh
Heat load	1132.66	808.02	MWh
Gas consumption	1569.13	1184.79	MWh
CHP electricity	423.53	318.48	MWh
CHP heat	784.56	592.4	MWh
SSR_{heat}	69.27	73.31	%
PV elec generated	51.04	105	MWh
grid electricity bought	430.39	243.51	MWh
excess electricity	231.54	196.75	MWh

Table 4.5: Summary of energy produced and consumed by the system. This table make the comparison between the mean and the robust optimal design.

the part of heat that is produced by the CHP unit. In the robust optimal design, SSR_{heat} is higher so the fact that gas_cost's Sobol index evolves in this way is normal. Reducing the uncertainties around these three parameters further helps to improve the system's robustness.

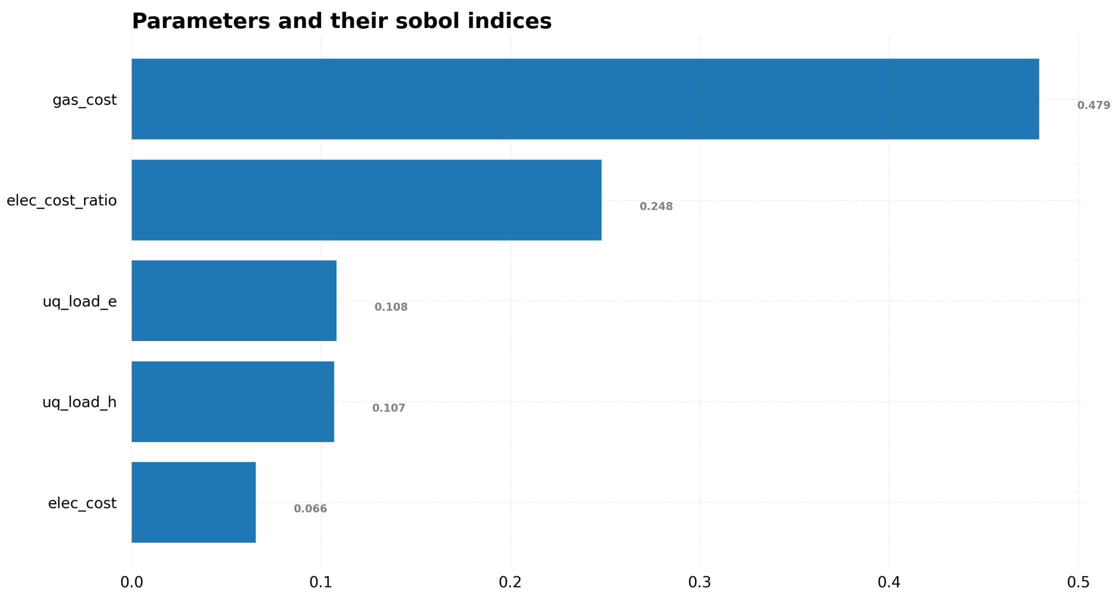

Figure 4.10: Sobol indices of **mean optimal design** when gas boiler is replaced by electric boilers. Gas_cost is by far the most influencal uncertain parameter. From lower mean optimal design. It is followed by the electrical grid uncertainty, the elec_cost_ratio and the elec_cost.

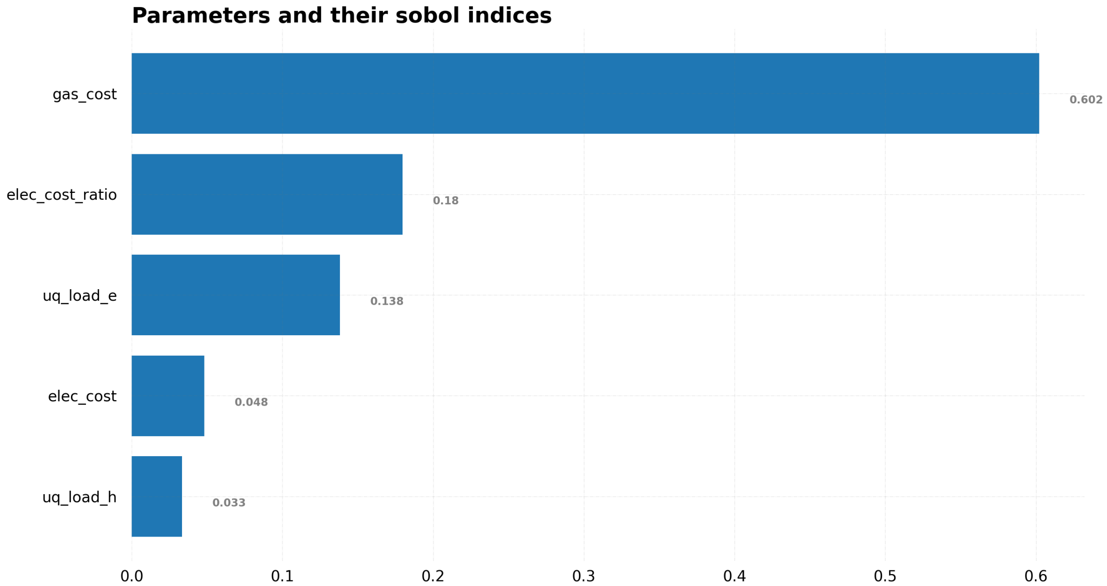

Figure 4.11: Sobol indices of **robust optimal design** when gas boiler is replaced by electric boilers. Once again, the uncertainty of this design is mainly driven by the gas_cost parameter. The inclusion of PV and batteries reduced the Sobol indicies of parameters linked to the grid (elec_cost and elec_cost_ratio).

Chapter 5

Piston engine connection

5.1 Theoritical recap

The original ICE (Internal Combustion Engine) was created in 1859 as a mean of converting chemical energy (fuel), into mechanical energy. The fuel is burned in a combustion chamber in the presence of high pressure air and results in a controlled explosion providing mechanical energy.

Technological improvements have increased the ICE's efficiency, largely by decreasing frictional losses in moving parts and improving the precision timing in the combustion process, where the air/fuel mixture is drawn into the chamber before being compressed, ignited, and exhausted (Figure 5.1). In addition, ICEs remain a common power source in the 21st century because of their adaptability, whether in the form of a reciprocating piston engine for automobiles and ships, or stationary applications in power plants where the engine's mechanical energy is converted to electrical energy through a generator.

The main components of an ICE CHP unit are as follows:

- the engine;
- the heat recovery system (exhaust gas heat exchangers and cooling water);
- the generator.

The engine: sizes for small-scale CHP systems can vary from around 25 [kW_e] output up to 500 [kW_e] very large diesel units. To match conventional electricity supply, the engines run at a multiple of the grid frequency (50 [Hz]), e.g. 1500 [rpm]. A typical internal combustion engine unit engine will run with a jacket temperature of 120 $°C$ and an exhaust gas temperature of 650 $°C$. The majority of heat is recovered from the exhaust gases. The temperature at which the engine runs is dependent upon a number of factors including engine speed and the fuel type.

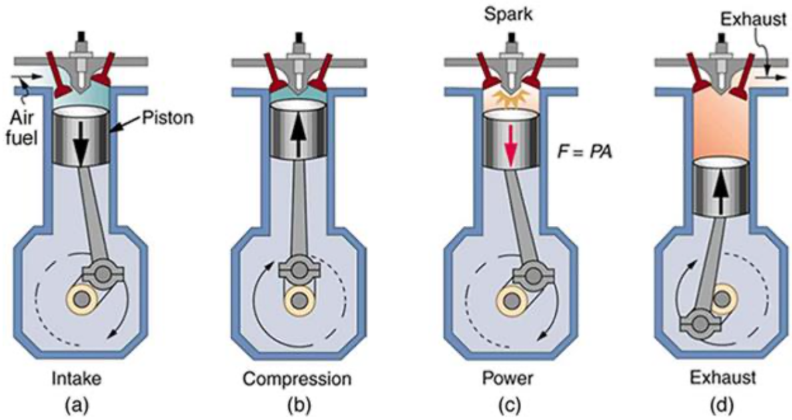

Figure 5.1: An internal-combustion engine goes through four strokes: intake, compression, combustion (power), and exhaust. As the piston moves during each stroke, it turns the crankshaft [34]

The heat recovery system: engine coolant water and exhaust gases are the two sources of recycled heat. Heat outputs for small-scale CHP units range from 39 [kW] to 1200 [kW] and are typically twice the electrical power output. The operating water temperatures are at approximately 75-90$°C$.

The generator: the basic components of the generator are the rotor and the stator. The rotor is the component driven by the mechanical torque from the prime mover, (i.e. the engine). The generators in packaged CHP units generally have a 3-phase alternating current output at 415[V] (line-line voltage), with a power output typically in the range 15 [kW_e] and upwards. Two types of generators can be used on CHP units: synchronous and asynchronous.

5.2 ICE unit and characteristics

2G Cenergy Patruus Series produces at nominal conditions 100 [kW_{elec}] and 143 [kW_{th}] with an electrical efficiency $\eta_{elec} \approx 35\%$ and a total efficiency $\eta_{tot} \approx 80\%$. As widely known, reciprocating ICEs have higher electrical efficiencies than MGTs. This is also obvious in the studied units: while the electrical efficiency of the 2G Cenergy amounts to 35%, the Turbec T100 is limited to 30% at nominal condition[35].
The part load electrical efficiencies and thermal power output for ICE unit are depicted in Figure 5.2.

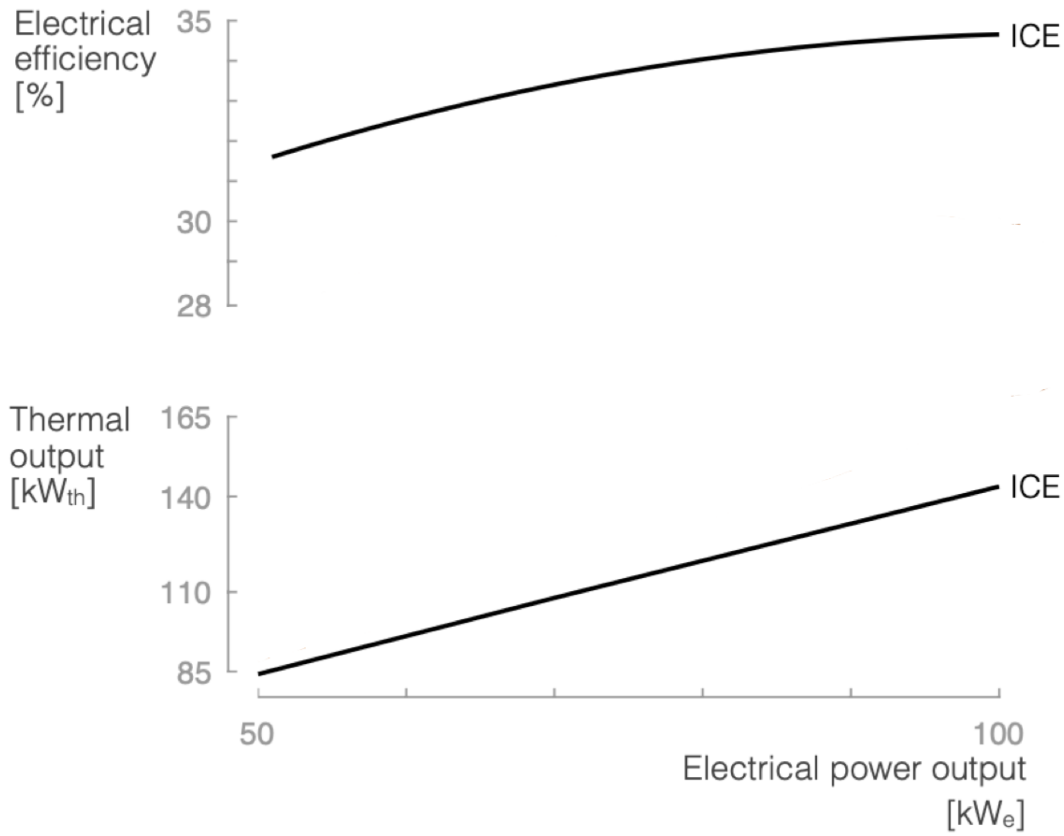

Figure 5.2: The ICE offers an electrical efficiency ranging from 30% to 35%. The cycle presents a thermal efficiency ≈ 50%. Data source: [35]

5.3 Modelization of the system

The system under investigation, see Figure 4.3, is exactly the same system as presented in Section 4.3 except that an internal combustion engine is installed, see Figure 4.3.

The system follows the same strategy as the one of the MGT, where the heat demand is the preponderant parameter. When the nominal power of the CHP(e.g. 143 $[kW_{th}]$ for the ICE) is lower than the demand, the cogeneration unit runs at **full load** and the remaining heat is provided by the boiler. Then when demand is between the nominal power and 50% of the nominal power of the CHP unit, it runs at **part load**. The generated power is compute thanks to the data given by the manufacturer, see Figure 5.2. Lastly, the demand is lower than 50% of the nominal power, the CHP is **shutdown** and the boiler fulfill the heat demand.

For the electrical demand, it is much more simple. The electricity is provided by photovoltaic panels, batteries and cogeneration unit. The CHP unit produces electricity only when it is running to comply with the heat demand. When the technologies installed are not sufficient, the system simply buy the remaining electricity from the grid.
Assumptions similar to the previous MGT-chapter were made. First, the effect of the ambient temperature on performance is not taken into account. Secondly, as for the whole study, they are no distinctions between space heating demand and dwelling heating water demand. Finally, the internal combustion engine has an expected lifetime of 50 000 hours of operation [35].
Figure 5.3 summarises the power strategy of present hybrid energy system.

5.4 Uncertain parameters

The Table 5.1 shows all the uncertain parameters related to the ICE. There are added to the parameters of the basic energy system in Figure 3.1.
The standard deviation σ of each parameter correspond to 5% of the mean value μ .

	Unit	Distribution	μ	σ	Range
$CAPEX_{ICE}$	$€/kW_e$	Uniform	2300	115	$[2185; 2415]$
$OPEX_{ICE}$	$€/kWh_e$	Uniform	0.0225	0.001125	$[0,02135; 0,02365]$
Unit lifetime	$Hours$	Uniform	50 000	2500	$[47500; 52500]$
Replacement costs	$€/kW_e$	Uniform	1700	85	$[1615; 1785]$

Table 5.1: Uncertain parameters of the ICE unit.

5.4.1 Investment and maintenance

The installation costs of the CHP unit include a variety of issues, such as the cost of the installation of the chimney, the cost of transporting the machine and the gas and electricity connection. Based on real cogeneration ICE machines currently operating in Brussels, these costs were estimated at 80 000 € for ICE unit [32].
O&M costs: as described in Table 5.2, ICE has higher O&M costs than MGT because it has more moving parts. So it requires specific lubricating oil (not contaminated with combustion products) in a higher quantity [32].

5.4.2 Lifetime of the unit

The lifetime (in years) of each technology depends on the running hours of the unit. For the ICE unit, it turns around 50 000 running hours, after that it would be

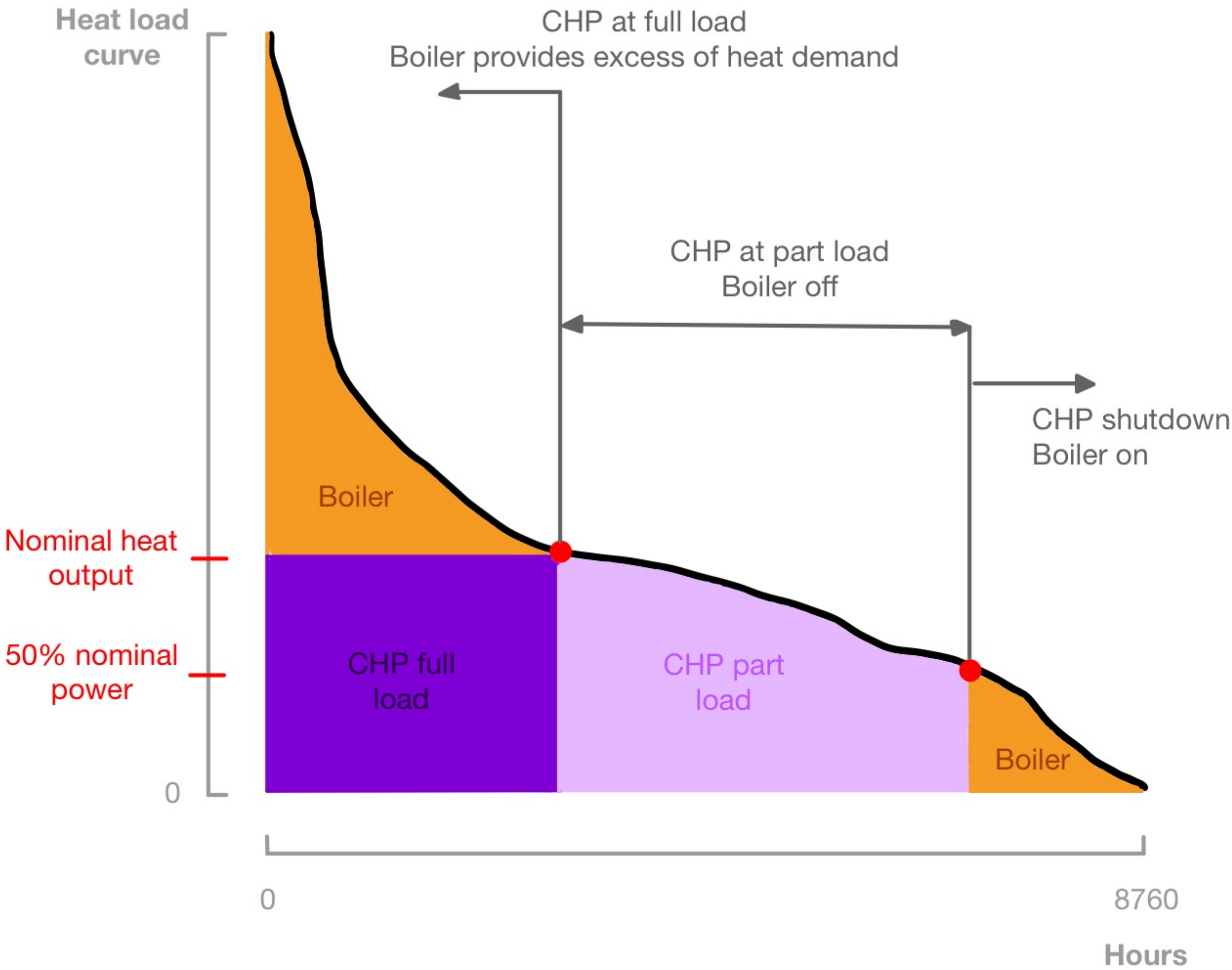

Figure 5.3: Heat load curve during 1 year (8760 hours). The system follows the heat demand, the electricity demand is covered by CHP, PV and battery (the lack of electricity is provided by the grid). When the heat demand is above the nominal power if the CHP unit, gas boilers provide the remaining heat. If the demand is between the nominal power and half of the nominal power of the CHP, it runs at part load. Under half of the nominal power, the cogeneration unit is shuted down and the gas boilers fulfil the demand.

	ICE	MGT
Installations cost	80 000€	80 000€
unit cost	150 000€	180 000€
O&M costs	0.015€$/kWh_e$	0.0225€$/kWh_e$

Table 5.2: Installation, capital and operation costs of the ICE and MGT

replaced because the O&M costs became more and more important [35].

5.4.3 Replacement costs

Replacement costs are common assumptions to the previous chapter as no informations on them were found. They are then quantified a bit lower than the CAPEX, see Table 5.1.

5.5 Quantity of interest and design variables

The design variables are the battery stack, the PV array capacity and the number of load, respectively n_{bat}, n_{pv} and n_{load} (in [kWh], [kWp] and [number of dwellings]). They are the same as in the MGT study.
The quantity of interest is the Levelized Cost Of eXergy (LCOX), presented in Chapter 3.

5.6 Results discussion

5.6.1 Scenario 1: not selling electricity, ICE-GasBoilers

The robust design optimization results illustrate the trade-off between minimizing the mean and minimizing the standard deviation of the LCOX, see Figure 5.4. The lowest mean (871.5 [€/MWh]) is achieved by a total of 33.7 kWp of PV arrays, 0.39 [kWh] of battery and a 14 dwellings. Reducing the LCOX standard deviation is then achieved by increasing the PV array capacity, followed by the inclusion of a battery stack and the reduction of the demand thanks to the number of dwellings design variable, Figure 5.5. This increase of technology installed reduces the dependency on the electricity price uncertainty.

	n_{PV} [kWp]	n_{bat} [kWh]	n_{load} [-]	μ_{LCOX}	σ_{LCOX}
mean optimal design	33.7	0.39	14	871.5	102.6
robust optimal design	43.6	66.3	10	904	97.9

Table 5.3: Characteristics of the mean optimal design and the robust optimal design

The system follow the same power strategy as the one with the MGT, so the heat is 100% provided by a gas consumption whose price is subject to a certain uncertainty. As before, the only way to reduce the impact of this parameter is to reduce the consumption of gas via n_{load} design variable, see Table 5.3. As you can see in Figures 5.6a and 5.6b, it is not sufficient because the gas price's sobol index stay constant between the mean optimal and robust optimal designs. Conclusion

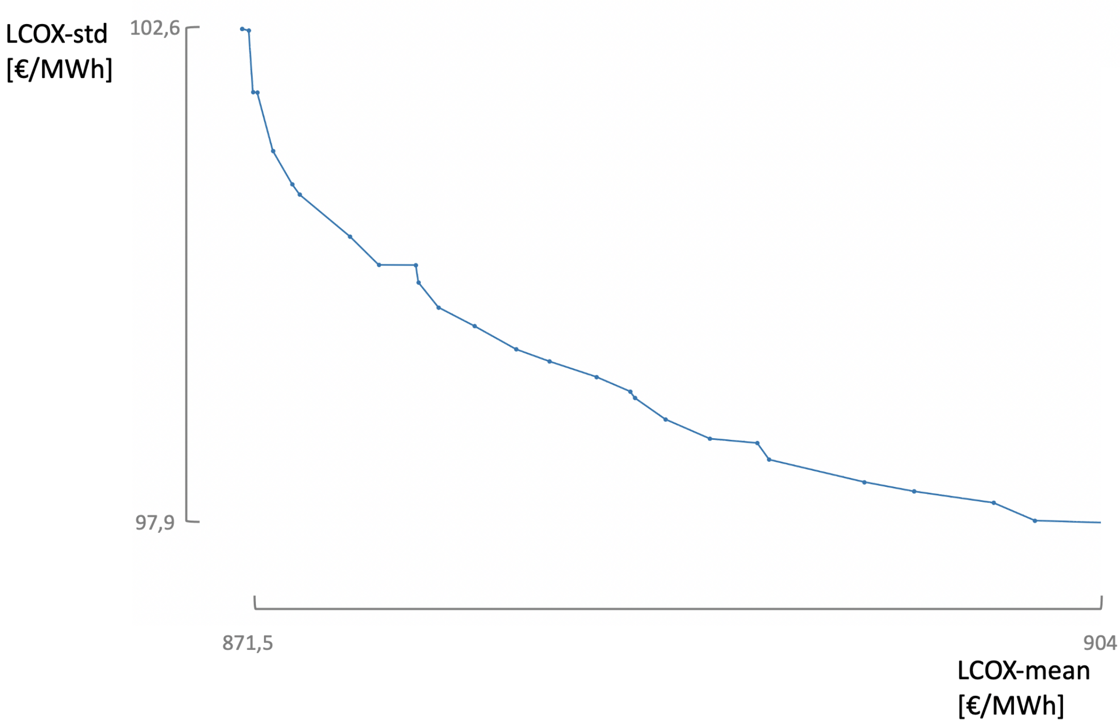

Figure 5.4: The Pareto front illustrates that a trade-off exists between minimizing the LCOX standard deviation and the LCOX mean. The increase of PV capacity installed and inclusion of battery stack will induce a decrease of the LCOX standard deviation.

is that the deployment of PV-battery has little effect on the LCOX-std as it only affects the amount of grid electricity consumed.

The Sobol' indices represented in Figures 5.6a and 5.6b clearly illustrate that the variation of the LCOX standard deviation is mainly due to the uncertainty on the gas price, the electricity load and the electricity cost ratio.

In this configuration, the CHP unit will cover only 0.9% of the heat demand. As presented in the micro gas turbine's section, this low number of households will reduce the total heat demand of the community and therefore shut down the ICE as much as possible, see Figure 5.3.
Considering this trend to annihilate gas consumption and desiring to exploit more the investigated technology, traditional gas boilers will be replaced by electrical ones in the next scenario.

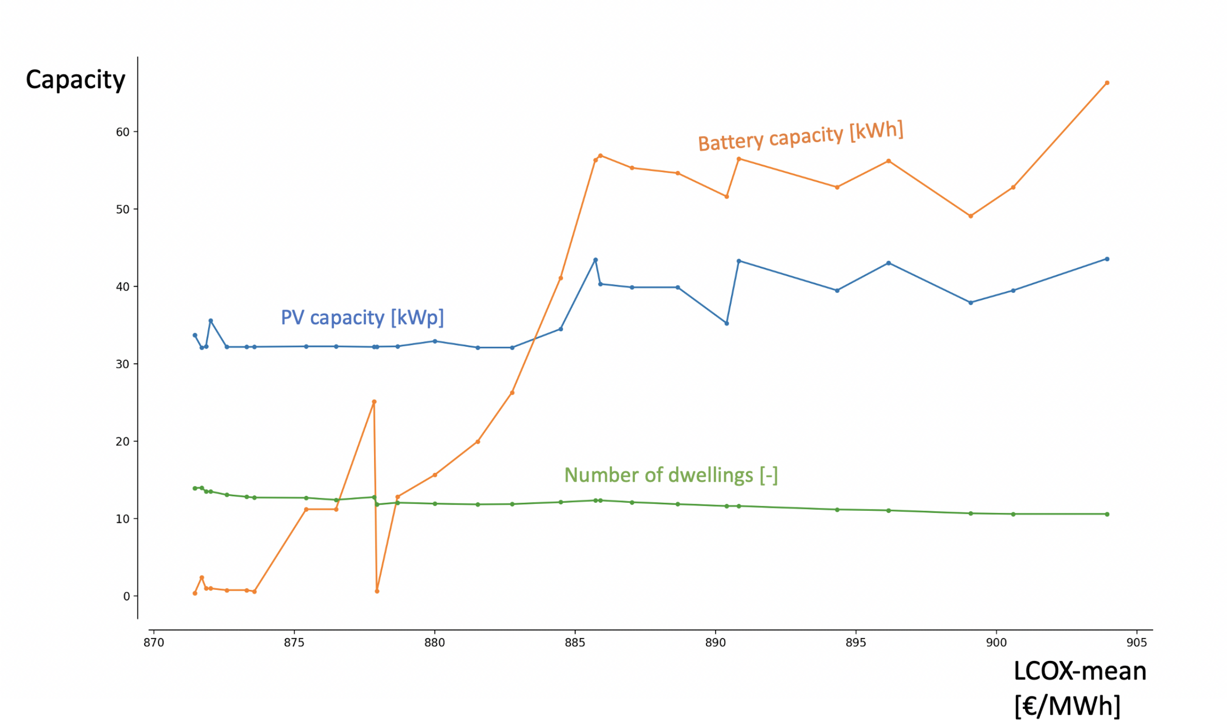

Figure 5.5: The evolution of the design variables when minimizing the LCOX's mean and standard deviation, in the PV-BAT-ICE-GasBoilers energy system. The PV capacity and the number of dwellings are quite constant, in the other hand there is an increase of the Battery capacity installed.

5.6.2 Scenario 2: not selling electricity, ICE-ElecBoilers

When the gas boiler is replaced by electrical boiler, the robust design optimization shifts the Pareto front (of the previous case) to the left and an increase of the LCOX's standard deviation (LCOX-std) is observed, see Figure 5.7. This strategy has an impact on the standard deviation of the LCOX, there is an increase of $\approx 16\%$ in the robust optimal design. Mean optimal designs comparison indicates 6% reduction of LCOX mean through the use of electrical boilers, Table 5.4.

Once again the philosophy is the same as the MGT case because it is the same kind of power generation, the only differences will be linked to the costs and some technical aspect but the difference is minimal in this complex energy system.
To pass from the mean optimal design to the robust optimal one, the optimizer will double the PV capacity and install batteries ($+215[kWh]$), as you can see in Figure 5.8 and Table 5.4. The insertion of PV-battery system reduces dependence on the electricity grid, for which prices are uncertain (elec_cost and elec_cost_ratio). As exposed in Table 5.5, this method drops the amount of electricity purchased by $\approx 150[kWh]$.

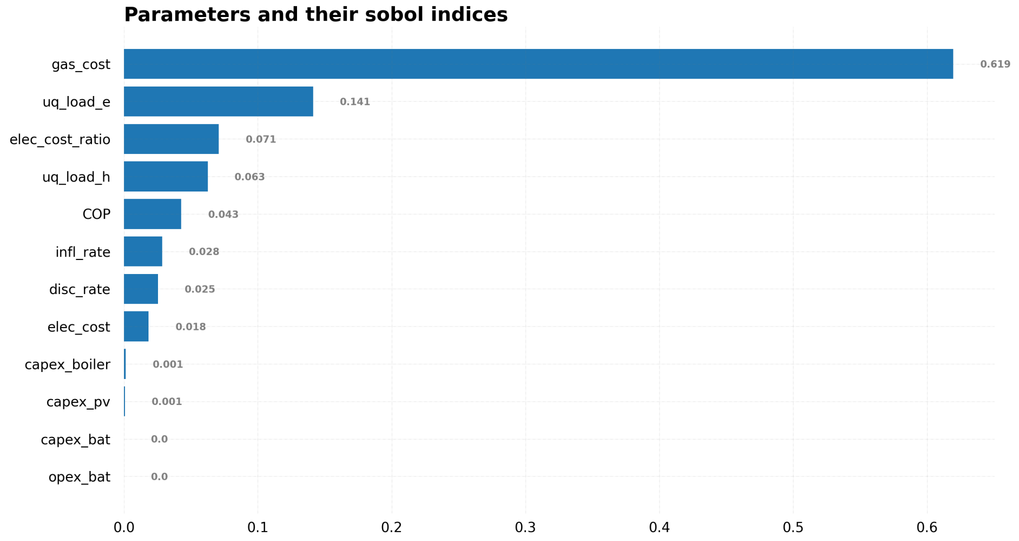

(a) Sobol indices of **mean optimal design**

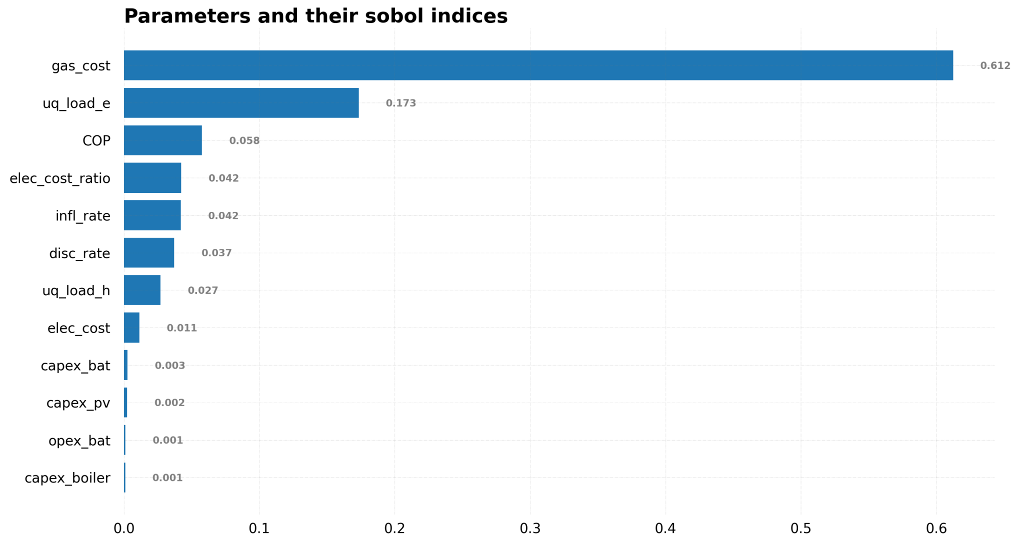

(b) Sobol indices of **robust optimal design**

Figure 5.6: Sobol indices of the main parameters of the PV-BAT-ICE-GasBoiler energy system. Two designs are presented here, the mean optimal(a) design and the robust optimal(b) design. The most uncertain parameter in this scenario is the gas_cost

Sobol indices evolution confirms this suggestion, Figures 5.9 and 5.10. As expected the ones related to grid electricity cost are decreasing. In the other hand, there is

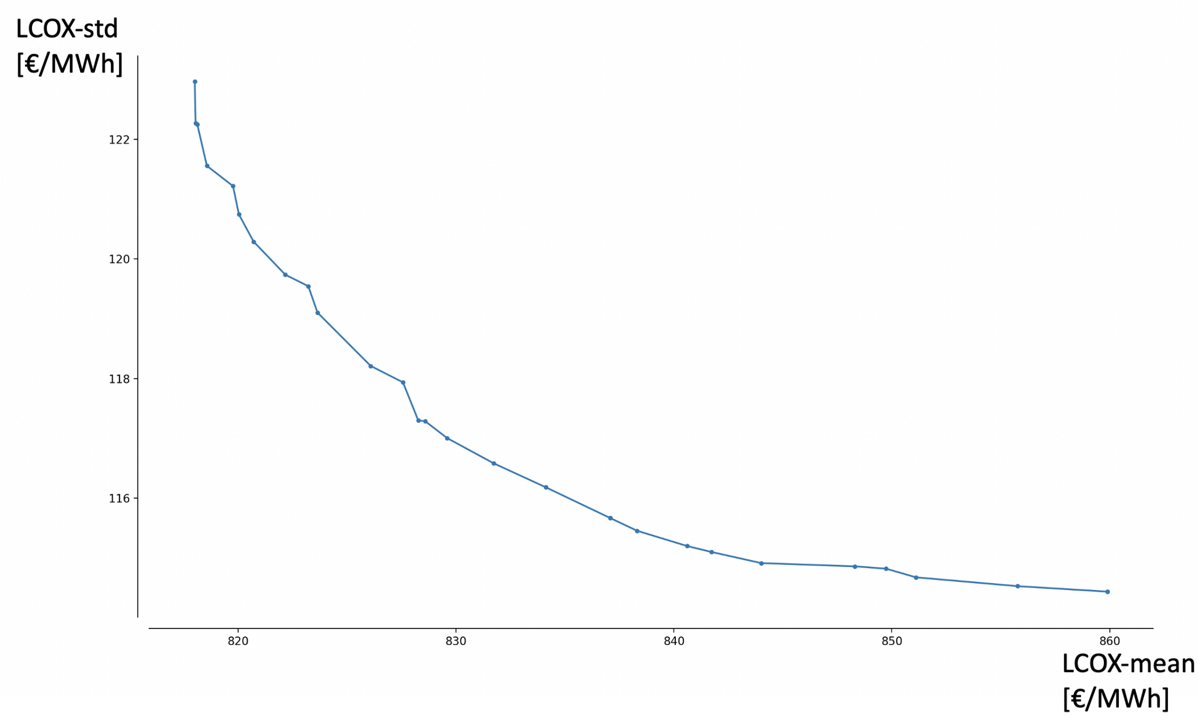

Figure 5.7: The Pareto front illustrates that a trade-off exists between minimizing the LCOX standard deviation and the LCOX mean. To pass from the mean optimal design to the robust optimal design, the optimizer will reduce double the PV capacity installed and avoid the dependency to the grid by including batteries. The number of dwellings DV will be reduced from 49.26 to 35.15.

an increase for the gas_cost Sobol index despite the diminution of the number of households (Table 5.4) and therefore the decrease of gas consumed by $\approx 340[MWh]$ (see Table 5.5). The explanation of this counter-intuitive evolution can be found in the Table 5.5 and more precisely in the SSR_{heat} values. It represents the amount of heat demand covered by the CHP unit, so an increase of the SSR_{heat} will induce an increase of the uncertainty coming from the gas price (gas_cost), as you can see in Figures 5.9 and 5.10. Reducing the uncertainties around these three parameters further helps to improve the system's robustness.

	n_{PV} [kWp]	n_{bat} [kWh]	n_{load} [-]	μ_{LCOX}	σ_{LCOX}
mean optimal design	44.75	0.97	49.26	818.08	122.96
robust optimal design	93.92	215.46	35.15	859.9	114.43

Table 5.4: Characteristics of the **mean optimal design** and the **robust optimal design** when gas boiler is replaced by electrical boiler in a PV-BAT-ICE energy system.

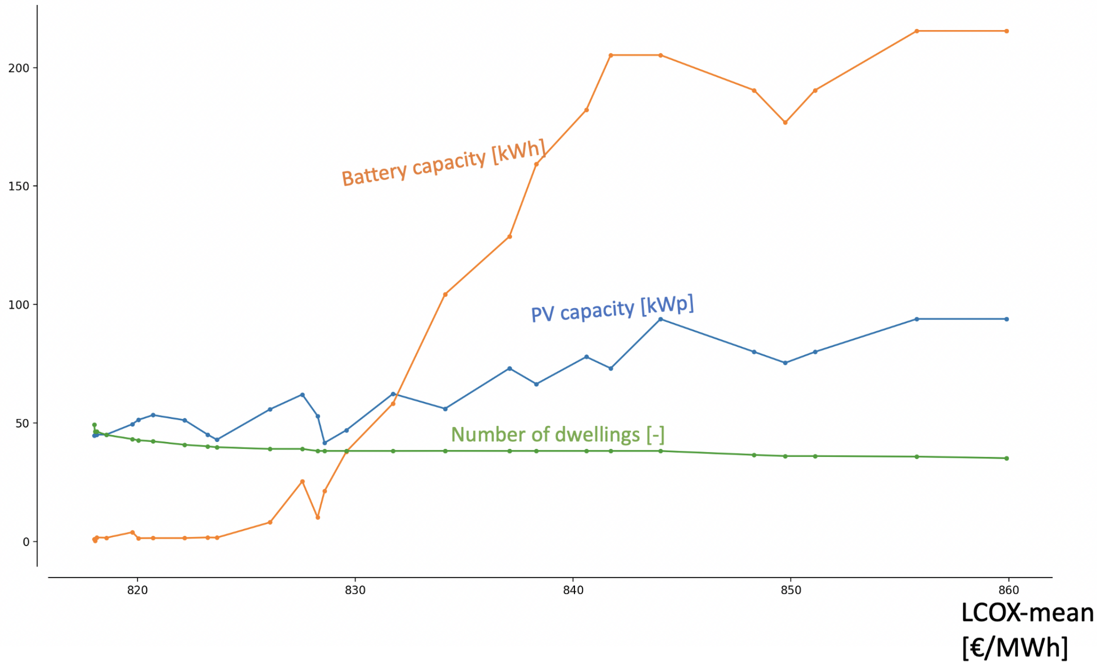

Figure 5.8: Evolution of the design variables when minimizing the LCOX's mean and standard deviation, in the PV-BAT-MGT-ElecBoilers energy system. The PV capacity and the number of dwellings are quite constant, in the other hand there is an increase of the Battery capacity installed.

	mean optimal design	robust optimal design	units
μ_{LCOX}	818.08	859.9	$€/MWh$
Elec load	215.74	153.95	MWh
Heat load	950.02	677.93	MWh
Gas consumption	1341.56	1002.9	MWh
CHP electricity	414.81	306.48	MWh
CHP heat	670.78	501.45	MWh
SSR_{heat}	70.61	73.97	$\%$
PV elec generated	39.23	82.34	MWh
grid electricity bought	348.76	200.29	MWh
excess electricity	245.93	196.09	MWh

Table 5.5: Summary of energy produced and consumed by the system. This table make the comparison between the mean and the robust optimal design for an hybrid energy system made of PV, batteries, ICE and electrical boilers.

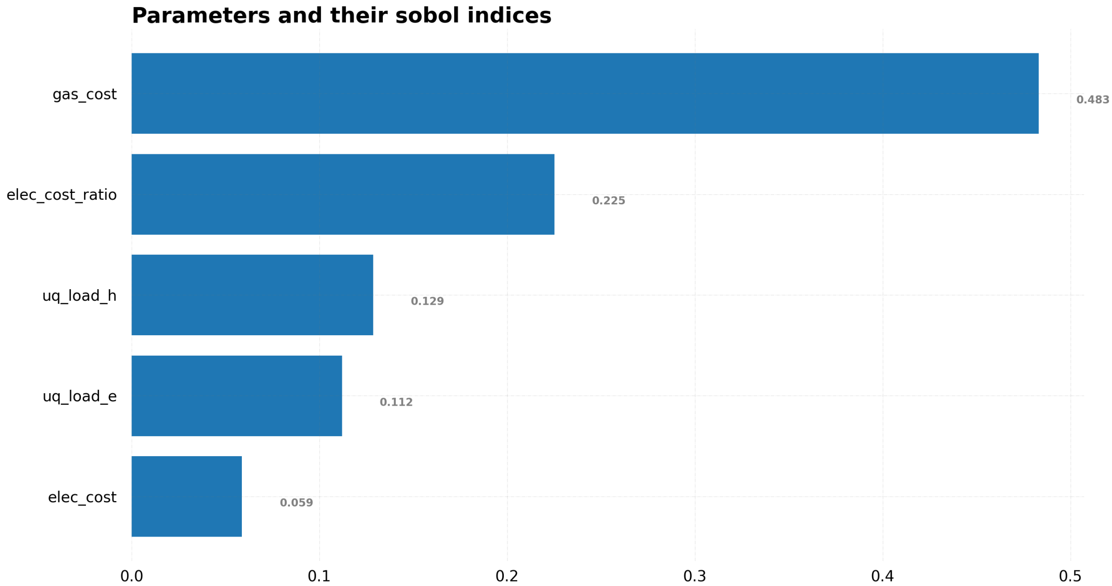

Figure 5.9: Sobol indices **mean optimal design** when gas boiler is replaced by electric boilers. Gas_cost is by far the most influencal uncertain parameter. From lower mean optimal design. It is followed by the electrical grid uncertainty, the elec_cost_ratio and the elec_cost.

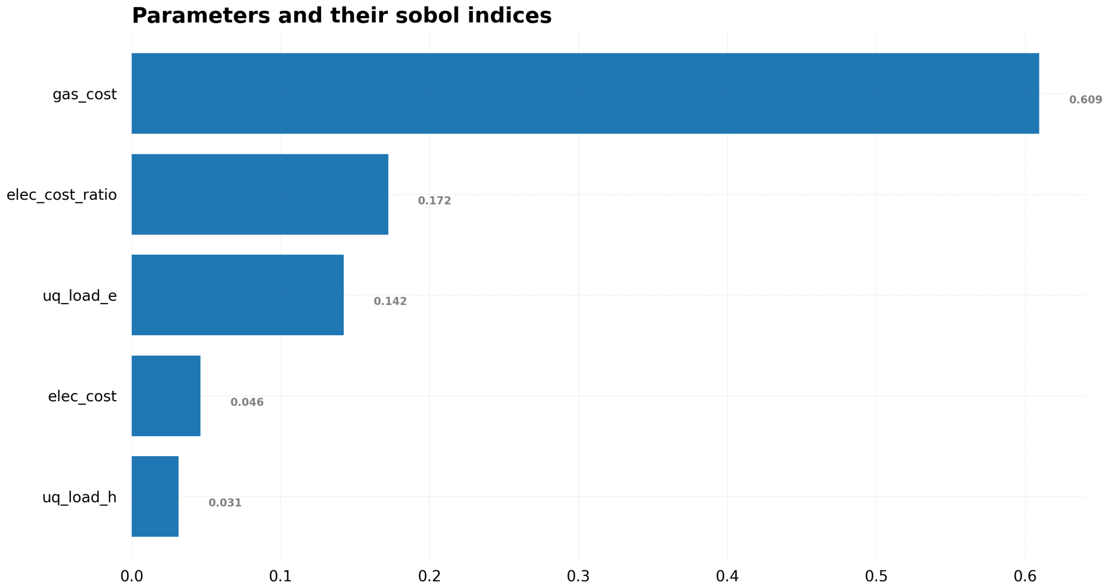

Figure 5.10: Sobol indices **robust optimal design** when gas boiler is replaced by electric boilers. Once again, the uncertainty of this design is mainly driven by the gas_cost parameter. The inclusion of PV and batteries reduced the Sobol indicies of parameters linked to the grid (elec_cost and elec_cost_ratio).

Chapter 6

Heat pump connection

The heat pump technology is the future of space heating. As residential space heating represents 13.3% of global emissions[36] in Belgium, the electrification through heat pump technology is an interesting part of the solution to lower carbon footprint.
At the moment, the technology is quite expensive and financial incentives are not convincing consumers to switch from fossil heating. However, tax incentives from 1000 € to 6000 € are already given in Wallonia, depending on household incomes. To switch from fossil fuels, some European markets have legislated against the gas connection of new housing or commercial buildings[37]. In Belgium, legal measures have been taken against oil fired boiler installations. Those are highly polluant and are largely spread within the country (50% of heating installations in Wallonia, 24% in Flanders and 16% in Brussels[36]). They want to get rid of the technology by 2035, blocking new installations from 2021. However, Belgium authorities do not want to precipitate gas banning thus further decisions will be made in the upcoming years on that matter[38].

6.1 Technology recap

Thanks to the circulation of a refrigerant fluid, a heat pump installation is able to inverse the classic heat sources exchanges. This particular type of fluid is able to absorb and deliver heat at uncommon states that allows to transfer heat energy from a cooler place to a warmer one. In this scenario, low-temperature state allows external air to be used as heat source, (down to minus 20 $°C$). The high-temperature state, reached with the help of an electric compressor, acts as heat source for the buildings to warm.

The standard way to characterize the efficiency of such installation is the *Coefficient of performance*(COP). It represents the heat energy delivered by the installation divided by the electrical energy provided in order to do so.

$$COP = \frac{Q_{spaceHeating}}{E_{compressor}}$$

As heat is captured in the surrounding air, the COP is higher than 1 and is temperature-sensitive. The COP commonly stays in the range of 2 to 8, depending on the technology and the quality of the equipment. Its value decreases with the external temperature as it represents a major heat source. In other words, let's assume that for the same heat to distribute, compressor work will be lowered if external air can provide higher proportion of heat at a higher temperature.

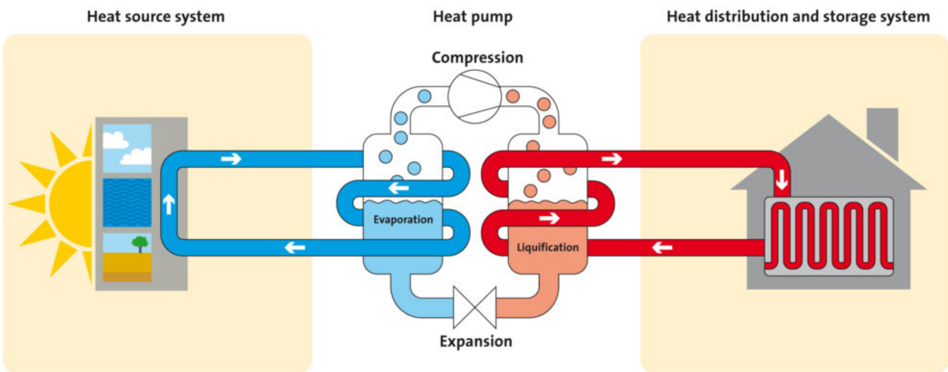

Figure 6.1: Heat pump heating mode schematic: the heat pump system is able to inverse Carnot cycle with the help of a circulating refrigerant fluid; it draws heat from an external **heat source system** that can be ambient air, body of water or underground pipes. The **heat pump** unit is made of four components allowing the refrigerant fluid to become a hot source in front of the demand. An evaporator and a condensator handle respectively the heat exchanges between the external heat source and the environment to heat. The use of an electric compressor induces an additional enthalpy rise of the refrigerant. Finally, the expansion valve lowers the pressures to turn the refrigerant to its initial state.

Heat pump unit components

Heat pumps are composed by four components:

- Heat is taken from the outside to evaporate the refrigerant fluid at low pressure (**evaporator**).
- The electric **compressor** heats up the refrigerant fluid to enhance its enthalpy and allows circulation though pressure difference.
- The heated gaseous fluid flows within a **condenser**, where it delivers heat to the demanding system. The fluid is then liquefied.

- Refrigerant is released in an **expansion valve** to lower the pressure to enable the cycle again.

External heat source systems

The external heat provided to evaporate the refrigerant is captured in the nearby environment of the installation. The most common way to do so is the surrounding air, with large temperature variations between seasons. However, to limit the variations and avoid major negative temperature drops in winter, one can install a grounded heat exchanger, at several meters of depth. In the context of this study, conventional and cheaper air-source heat pump is used.

6.2 Modelling of the heat pump energy system

To develop numerical computations and their analysis, a numerical Python model has been made. In order to combine precision and efficiency, some assumptions have been made at many levels of the energy system. This subsection will explain and justify them.
The following Figure (6.2) illustrates the simple model of heat demand met through a variable speed heat pump, assisted by an emergency electrical boiler ($\eta_{elec->heat} = 0.9$). The electrical boiler has an unlimited power potential but for the aim of the analysis, it will not reach unrealistic values. As its use is in any case energetically less efficient, the optimizer will naturally explore designs where its contribution is not preponderant.

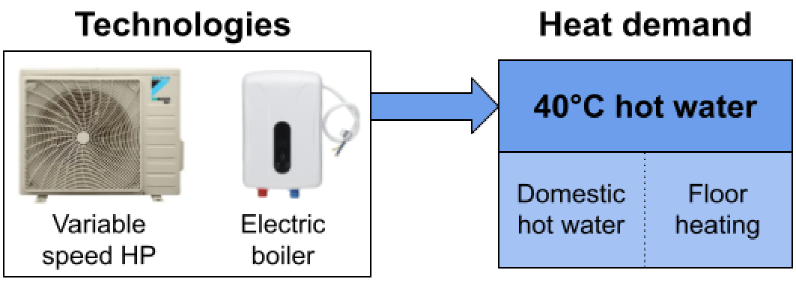

Figure 6.2: Heat demand satisfaction in heat pump model. Two heat production technologies ensure the fulfill of the demand. The heat demand is characterized by hot water at 40 °C, serving both domestic hot water needs and space heating through floor heating systems.

Heat production technologies distribution

The model evaluates how the demand will be satisfied every hour. The distribution between the heat pump installation and the electrical boiler depends on the performance of the heat pump and how it can fulfill the demand. As the COP is temperature sensitive, the heat pump potential is variable and three values are hourly determined:

- Q_N [Wh]: maximal calorific energy when heat pump works one hour at nominal electrical power.
- Q_{30} [Wh]: heat delivered when heat pump works one hour at 30% of nominal electrical power (lower inverter limit)
- $Q_{30_{10m}}$ [Wh]: heat delivered when heat pump works during 10 minutes at 30% of nominal electrical power. This limit is fixed to avoid launching the installation for very low demand and short amount of time(on-off starting limit). Below this limit, the system favours the electrical boiler.

The Figure 6.3 shows how those values are used to determine which heat source is activated. The variable speed heat pump may have 4 different states:

1. Inactive: the demand is below $Q_{30_{10m}}$ and the boiler handles it.
2. Variable time: the HP works less than one hour (and >10minutes) at lowest rate (30% of electric nominal power).
3. Variable speed: the HP unit works for an hour at modulated speed between 30% of nominal power and nominal power W_n.
4. Nominal: the demand is above the heat pump maximal output thus handled both by the heat pump at nominal power and the electrical boiler.

Characterisation of the demand

The demand is represented as an hourly need by an household. To simplify the model, there are no distinctions between space-heating and domestic hot water, considering that they are both circulating at 40 $°C$. The absence of a heat storage tank can be justified by the ability of the variable speed heat pump to smooth the demand thanks to its inverter. The following Figure(6.4) illustrates the distribution of the heat production between a $3.5kW$ heat pump and the electrical boiler, following the rules defined earlier.

The heat pump is able to satisfy 93.7% of the calorific demand at an average COP of 3.41. During the summer months, lots of heat production is attributed to the boiler due to lower need. During spring and autumn, the ability of multi-speed heat pump allows to continuously smooth the demand and involves lower boiler use. In winter, when the performances of the heat pump installation are declining, the boiler is often coupled with nominal HP running to meet the demand.

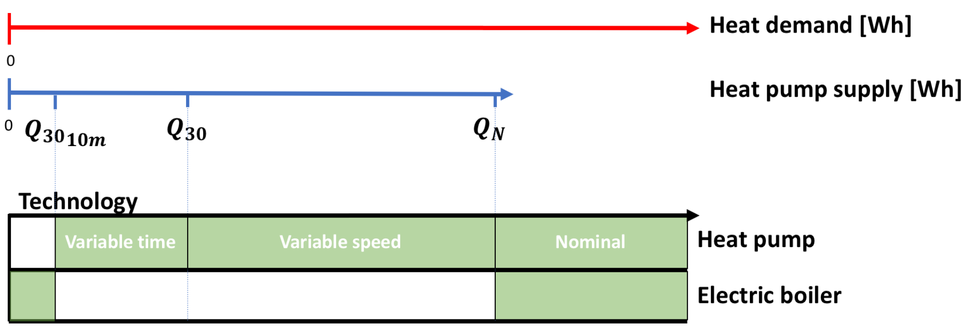

Figure 6.3: Choice of heat production technology vs demand. The heat pump has four possible states of working, depending on the heat demand. For two of them, the additional use of the electrical boiler ensures the demand satisfaction. First, when the demand is very low, the heat pump is preserved from on-off starting that may harm the technology. Secondly, the electrical boiler provides additional heat when the heat pump can not match demand at maximal power. In between, the heat pump can both work at minimal regime during a variable amount of time or during one hour at a modulated power.

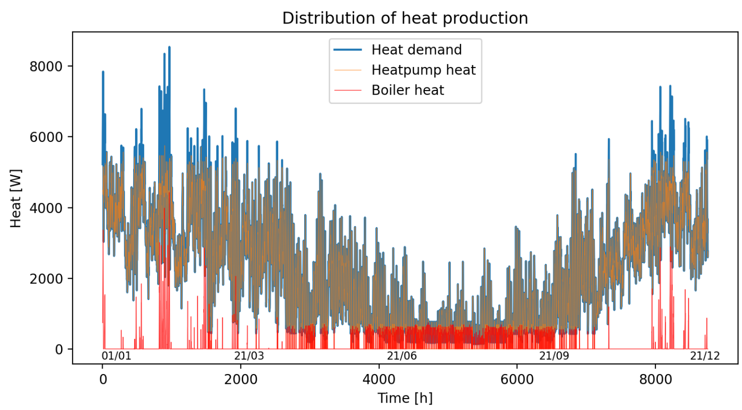

Figure 6.4: Distribution of heat production between a 2[kWe] HP and an electrical boiler for one household. When the demand is very low (mostly in summer), the HP is preserved from on-off starting and demand is met by the boiler. In colder periods, when the demand is higher and COP is getting worse, the electrical boiler frequently helps to match the heat demand. The rest of the time, the modulating speed ability of the HP ensures perfect matching between demand and production.

6.3 Heat pump unit and characteristics

To approach realistic values, the HP unit performances and characteristics are retrieved from an existing air-water low temperature model from company *Daikin*, (model *Altherma M*, ERHQ-BV3 [39]). The choice of an air-water heat pump allows to mingle domestic hot water and space-heating supply, circulating at the same temperature of 40 $°C$.

6.3.1 Extreme states

Hot source: to obtain circulating water temperature of 40 $°C$ assuming a temperature pinch of $\Delta T_{pinch} = 5°C$ at the condenser. The high temperature $T_{condenser}$ of refrigerant fluid hot source is thus 40 $°C + \Delta T_{pinch} = 45°C$.
Cold source: the technology offered by Daikin allows to work at extreme temperatures down to -20 $°C$. As temperatures in Brussels do not go under -7 $°C$, the lack of performance due to freezing conditions is not taken into consideration.

6.3.2 COP performance map

2006 KUL interpolation

The performance of the air-water heat pump are based on the work of *KUL* researchers in 2013[40]. They have developed a variable speed air-water *Altherma* heat pump model and developed its COP map for different modulation levels. The different levels are 30% of the nominal power, the lower limit of utilisation of the technology, 50%, 90% and the nominal power W_N. They have based their analysis on the datasheet of a 2006 model of which the performance map is drawn in the following Figure(6.5). The data points are based on the datasheet from the company for 3 different condenser temperatures (30 $°C$, 40 $°C$ and 50 $°C$) with a modulation level mod_{level} from 30% up to nominal power.

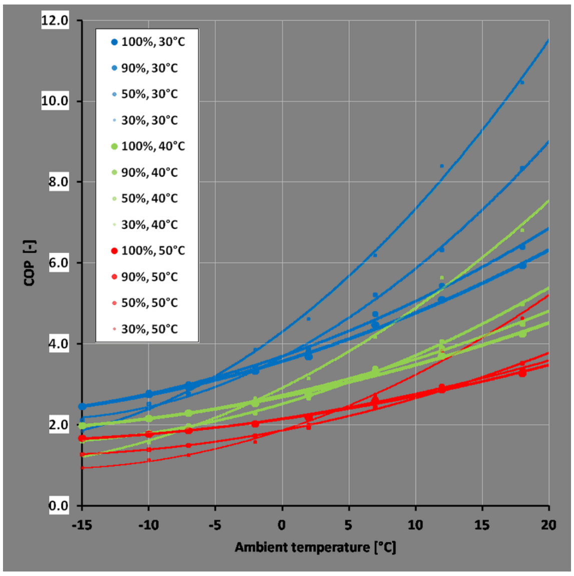

Figure 6.5: KUL mapping points: the performances of the HP are based on a study from KULeuven in 2013. The heat pump model was an air-to-water variable speed model from the company *Daikin*. They have mapped the COP for several maximal temperatures of the refrigerant fluid (T_{cond}) and modulated regimes. For the aim of the thesis, those points have been interpolated to obtain a numerical mapping of HP behavior.

As the condenser temperature is 45 $°C$, the mapping has been linearly drawn between 40 $°C$ and 50 $°C$ results. The data points of the figure here over have been retrieved thanks to an online plot digitalizer[1] and interpolation has been performed to get the values of the COP ($COP = COP(mod_{level}, T_{ext})$) for each condenser temperatures and over the working range($[30\% W_N; W_N]$). Those two steps (interpolation + average) allowed to get a similar function for the COP of the heat pump unit, for a condenser temperature of 45 $°C$.

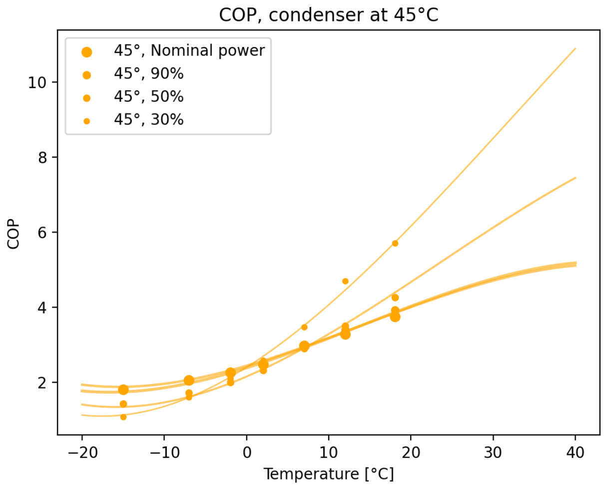

Figure 6.6: Interpolation functions when $T_{cond} = 45°C$. Assuming a temperature pinch of 5 $°C$ while supplying the necessary 40 $°C$ to meet the demand, the condenser temperature of the unit is fixed at $45°C$. To interpolate the mapping at this temperature, a linear average has been done between $T_{cond} = 40°C$ and $T_{cond} = 50°C$ from the KUL mapping.

Step-up of technology

As the interpolation work has been done for a 2006 unit, an amelioration of the technology along with better performances could be expected and thus better performances. In fact, based on the datasheets ([41] and [39]) and a telephone exchange with the company, the HP treated by the KUL is a prototype of the Altherma units that are marketed nowadays. Besides several changes on material choices and design, the performances are the same as the compressor, the fluid and the condenser have not been changed. Thus, the COP mapping is perfectly equal from one unit to another.
However, uncertain parameters have been established on potential improvement of HP technology.

[1] https://automeris.io/WebPlotDigitizer/

6.4 Uncertain parameters

Apart from the parameters of basic energy systems introduced in the previous sections, several ones are specific to heat pump technology. Table 6.1 is a resume of all 5 of them. Their characterisation is developed after.

	Unit	Distribution	μ	σ	Range
$CAPEX_{hp}$	$€/kW_e$	Uniform	1100	150	$[950; 1250]$
$OPEX_{hp}$	$€/kW_{th}/year$	Uniform	5.5	1.8	$[3.7; 7.3]$
Technologic step up	%	Uniform	8	8	$[0; 16]$
Unit lifetime	$Year$	Uniform	20	5	$[15; 25]$
Replacement cost	€	Uniform	4500	1500	$[3000; 6000]$

Table 6.1: Heat pump uncertain parameters

6.4.1 Investment and maintenance

Capex

To determine the investment cost of the heat pump technology, a parallel can be made with the air-water *Alterma* model. As the demand of one household does not exceed $13kW_{th}$, the pricing analysis is based on two units delivering heat power in this range. The pricing of the units and their respective CAPEX are presented in the following table (source: Daiking pricing catalogue [42])

The pricing is the following:

Peak power [kWe]	Total price [€]	Capex [€/kW]
4.4	5480	1250
7	6690	956

Table 6.2: Pricing and capex for two adapted units.

The uncertainty on heat pump Capex has been uniformly distributed between 0.956 and 1.25 [€/W]. The lower limit anticipates potential democratisation of the technology through incentives. Concerning the upper limit, even if the CAPEX decreases with the nominal power, it may still take into consideration potential price rises or more expensive models developed by concurrents.

Opex

The OPEX data are taken from Cao et al.[43] on which a correction factor is applied as more expensive technology is used (uni-speed vs variable speed HP). The correction factor is identical as the one between the Capex average value and the one from their work.

μ_{capex} from [43]	Altherma μ_{capex}	Difference
842	1103	+31%

Table 6.3: Average difference of pricing between uni-speed and variable speed units

Translating this difference of CAPEX to the OPEX, the mean value of Cao et al.[43](5.5[$€/kW_{th}/year$]) is risen up to $5.5 + 31\% = 7.205$. The variance of the uniform distribution has not been re-evaluated. This leads to an uncertain parameters on the HP OPEX distributed from 5.4 up to 9 [$€/kW_{th}/year$].

6.4.2 Technological step-up

Karellas et al.[44] studied the amelioration of heat pump performances with energy recovery at the expansion valve. Schematically, it can be represented as the figure below (Figure 6.7):

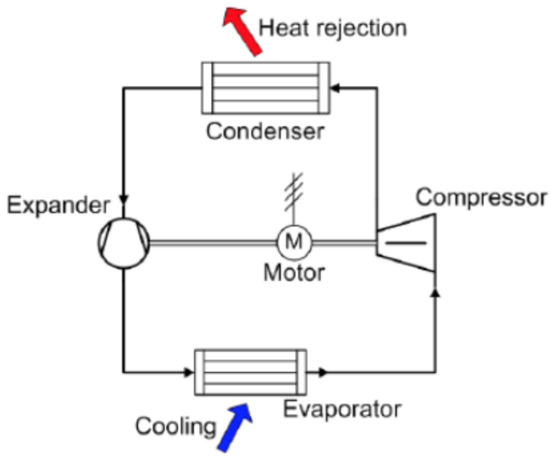

Figure 6.7: Representation of an HP COP-improvement by Karellas et al.[44].
The expansion work within the expander is retrieved from the compressor. Those savings limit the work of the compressor motor and thus enhance the global performance of the system.

Smart connection between compressor and expander allows energy recovery which thus lowers the use of mechanical work at the compressor motor. Their results for such method is exposed in the following figure (6.8), for a T_{cond} of $60°C$. As *Daikin Altherma* model is working with a R-410a fluid, the curve of interest is the one highlighted in red.

From this, the assumption of a linear potential enhancement of the COP is dressed, in accordance with the highlighted line. The linear interpolation for a wider range of temperature is shown in the following figure (fig 6.9).

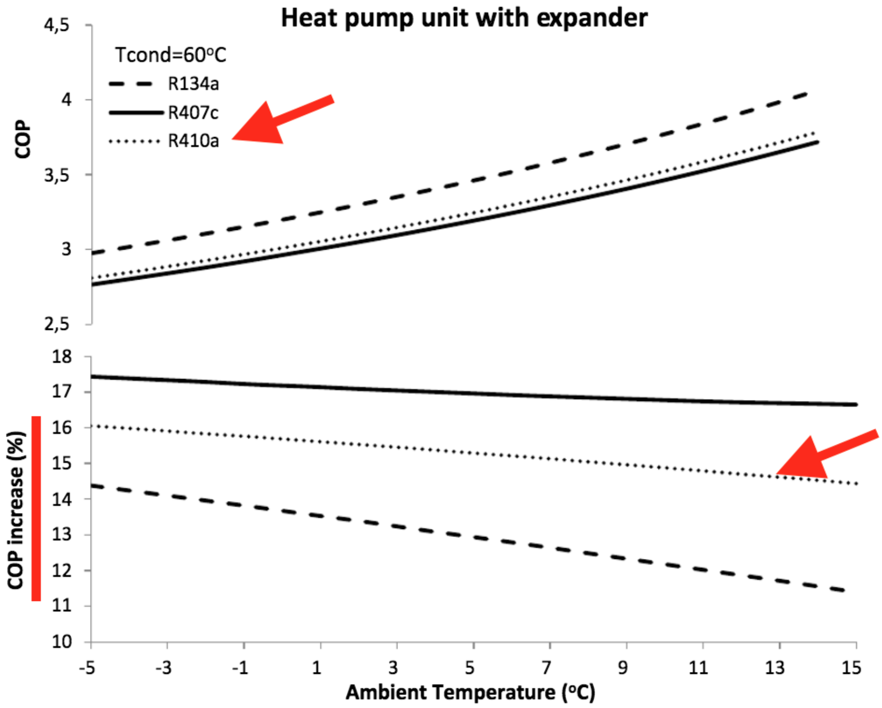

Figure 6.8: Amelioration of the COP for several frigorific fluids (from [44])
The highlighted parts are the information of interests. It shows the potential COP improvement for the same fluid of the *Daikin Altherma* model. The curve seems to evolve linearly and is decreasing with the ambiant temperature.

As this technology still encounters technical issues at the compressor-expander link, the uncertainty is uniformly distributed from 0% (no amelioration at all) to 100%(marketable technology, potential confirmed) of the improvement potential represented by the line.

The fact that it has been made for T_{cond} of 60 $°C$ does not allow to see bigger amelioration as work retrieved would be higher for hotter temperatures. However, this upper limit is kept to take into account the potential of other amelioration methods over time and see how it could impact the optimization of the energy system.

6.4.3 Lifetime of the unit

According to many sources, the expected lifespan of heat pump is from 10 up to 25 years[2]. It is also widely said that nowadays technology is getting more and more robust. For that reason and considering variable speed HP unit(hazardous on-off cycle avoided thanks to the inverter technology), the range is cut from 15 up to

[2]https://termo-plus.com/blog/life-expectancy-of-heat-pumps/

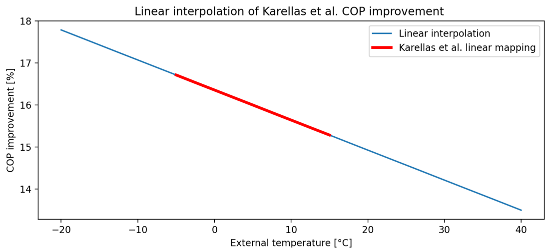

Figure 6.9: Linear interpolation of COP improvement potential.
Assuming that the improvement curve of figure 6.8 is linear, a quick mapping draws the following line, for a wider range of temperature.

25 years. A uniform distribution is established between 15 and 25 years for the uncertainty on the lifetime of a unit.

6.4.4 Replacement costs

Informations from [45] allows to draw a uniform distribution for the replacement costs. As this parameter is highly uncertain following the nature of the failure, the range is quite large (3000€ - 6000€). However, the replacement cost can not be higher than the price of the initial investment $CAPEX * P_{nom}$.

6.5 Results & discussion

In the following section, several scenarios have been investigated. The first two are common to the previous chapter and involve opportunity of selling the electricity back on the grid. However, using the demand profiles of one household, the optimized results for the heat pump nominal power are quite irrelevant. For both scenarios, the heat pump electric nominal power of optimized designs fluctuates between 3 and 4.2 [kWe]. First, this range is small for variable speed units. The smallest commercial units prices start around 4.5 [kWe] maximal electrical power. Secondly, as the size (and thus the price) of the unit is small, uncertainties specific to the heat pump do not have significant impacts. A third and fourth scenario have thus been investigated where the heat pump power has been fixed to the minimal commercial units (Daikin 4.4 [kWe] unit). The third scenario search for robust optimums of technologies for a fixed demand. The fourth will include the load in the design variables, to look for the ideal load and PV-battery distribution for one unit.

6.5.1 Scenario 1: PV-battery-HP not selling electricity

The robust design optimization results illustrate the trade-off between minimizing the mean and minimizing the standard deviation of the LCOX, see Figure 5.4. The lowest mean (638.6 [€/MWh]) is achieved by a total of 4.6 kWp of PV arrays, 0.4 [kWh] of battery and an HP electric nominal power of 1.9 [kWe]. Reducing the LCOX standard deviation is then achieved by increasing the PV array capacity, followed by the inclusion of a larger battery stack. This increase of technology installed reduces the dependency on the electricity price uncertainty. However, as HP thermic potential rapidly matches heat demand, the design variable on HP nominal power does not vary that much. As mentioned previously, this range of heat pump unit nominal power does not match any existing commercial technology. One could say that this scenario is not feasible at the moment.

	n_{PV} [kWp]	n_{bat} [kWh]	n_{hp} [kWe]	μ_{LCOX}	σ_{LCOX}
mean optimal design	4.6	0.4	1.9	638.6	175.7
robust optimal design	17.5	18.8	2.8	883.2	111.7

Table 6.4: Not selling: characteristics of the mean optimal design and the robust optimal design

6.5.2 Scenario 2: PV-battery-HP selling electricity

When the sale of electricity is possible and taken into account, the LCOX's mean of the optimized population is slightly reduced due to the possibility of earning money back. Moreover, the LCOX's variance is also reduced. The most robust cases for both scenarios are $\sigma = 103$ if selling is possible and $\sigma = 112$ otherwise. This increase of robustness is due to the augmented reliance on PV-panels production unit due to the opportunity of selling electricity. It enhances the SSR of the system which thus avoids buying electricity at uncertain cost. The Sobol indices testifying of the most significant uncertain parameters confirms that *cost ratio* value deeply influences the global robustness of the system (figure 6.11)

	n_{PV} [kWp]	n_{bat} [kWh]	n_{hp} [kWe]	μ_{LCOX}	σ_{LCOX}
mean optimal design	7.6	0.004	2	619.34	162.4
robust optimal design	20.7	20.4	2.67	833.6	102.7

Table 6.5: Characteristics of the mean optimal design and the robust optimal design

6.5.3 Scenario 3: Fixed HP unit, one load

For this scenario, the maximal power of the heat pump is equivalent to the minimal commercial unit (Daikin air-water low-temperature unit, running at 4.4 [kWe] maximal power). Compared to the previous scenario, the LCOX rises due to the oversized HP-unit. Concerning the robustness, there is a slight difference between the two

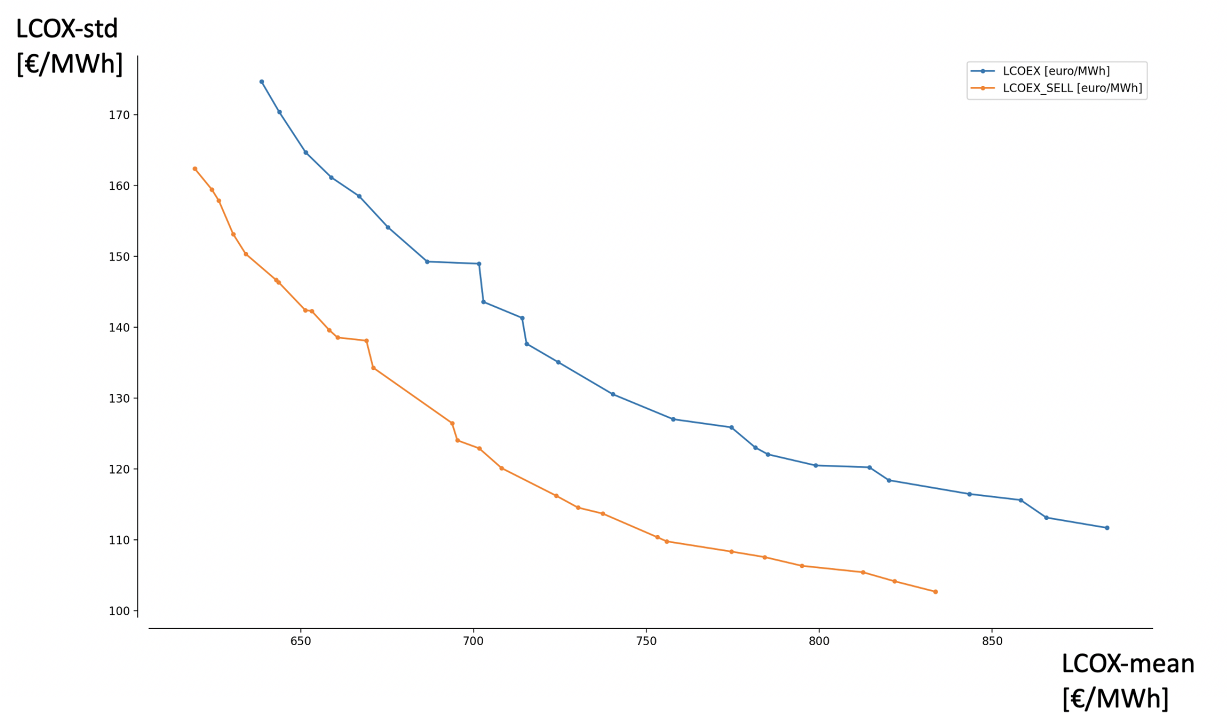

Figure 6.10: Pareto fronts comparison between selling and not selling scenarios
As the Pareto front of the selling scenario (in blue) moves both left and down, selling electricity seems beneficial to reduce LCOX mean value and variance of LCOX.

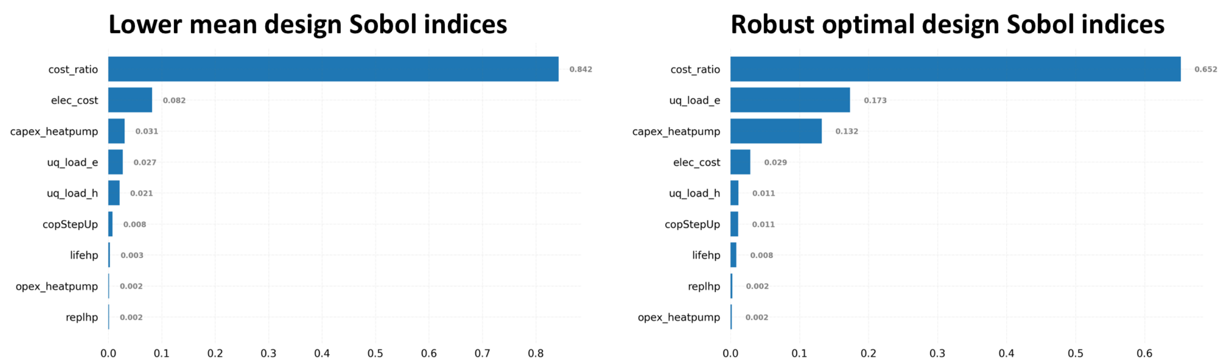

Figure 6.11: Significant Sobol indices for most optimal designs of selling scenario.
Cost ratio is by far the most influential uncertain parameter. From lower mean optimal design to robust optimal one, its impact is slightly reduced. This reduction is due to the increasing Pv-panels installation that makes the system more self-sufficient in the matter of electricity. It thus reduces the need of grid electricity at uncertain cost.

scenarios for the most robust optimized design. Those differences are indexed in the following table (6.6). Their analysis is provided on a case-by-case basis below.

	$\boldsymbol{\mu_{LCOX}}$ **range**	$\boldsymbol{\sigma_{LCOX}}$ **range**
Scenario 2: selling	[619-834]	[103-162]
Current scenario	[685-925]	[105-169]

Table 6.6: Comparison between selling scenario and current scenario.

Mean optimal design

	n_{PV} [kWp]	n_{bat} [kWh]	n_{hp} [kWe]	μ_{LCOX}	σ_{LCOX}
mean optimal design	7.1	0.01	**4.4**	684.84	168.8

Table 6.7: Characteristics of the mean optimal design.

First, it is important to recall that HP-unit does not produce heat if the hourly demand is lower that $Q_{30_{10m}}$ (heat energy production at 30% of maximal power, during 10 minutes). If the HP-unit is oversized, more situations like this occur. In comparison, for the same situation, the optimized unit of scenario 2 will run 4915 hours and provide 94% of the heat. For a 4.4[kWe] HP-configuration, the unit runs 3516 hours and feeds 91.2% of the heat demand. As this difference takes place when the low-efficient boiler is requested, it has significant impact on the system.
In the low mean optimal design, the system relies more on the electrical grid which is highly subject to uncertainties. The worsening of the robustness is due to a bigger boiler use, thus more call on uncertain electrical grid energy (see Sobol indice on *cost ratio* on figure 6.12).

Robust optimal design

	n_{PV} [kWp]	n_{bat} [kWh]	n_{hp} [kWe]	μ_{LCOX}	σ_{LCOX}
robust optimal design	23.56	23.53	**4.4**	925	104.4

Table 6.8: Characteristics of the robust optimal design

When comparing the selling scenarios on Table 6.8, the mean value of the most robust design soars while its variance is unchanged. As most of the analysed results, the uncertainty on bought grid electricity plays a major role in the evolution of the optimized population. The oversized unit involves a greater use of the electrical boiler, which results in a greater need of electricity. To switch from this situation to a more robust one, the optimizer will improve the self-sufficiency with more PV-battery installations. This will enhance the global cost of the system. Coupled to

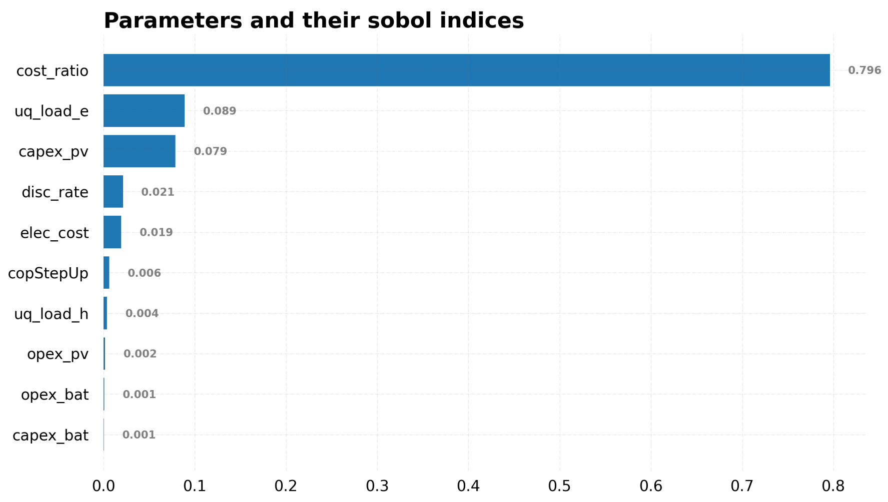

Figure 6.12: 4,4 HP-unit for one load, lower mean design Sobol indices: the *cost ratio* is the most dominating uncertain parameter as it highly influences the price of bought electricity. In the case of an oversized HP-unit, the range of operation is risen up as it can provide more heat. For low demand, the electrical boiler will thus be more often requested. As this heat production method is less efficient, the required electricity is higher and deteriorates the robustness due to its uncertain trend.

the oversized HP investment, it explains why the LCOX mean value soars. Regarding the robustness, the following figure (6.13) allows to determine what are the most impacting uncertain parameters. The gain on robustness from *cost ratio* Sobol indice reduction is compensated with a loss on several other uncertain parameters such as the electrical demand adapting factor and costs of PV-battery installations.

6.5.4 Scenario 4: Fixed HP unit, variable load

This scenario has been investigated to question what could be the ideal load for an actual commercial HP unit with current characteristics (air-water, low temperature). As the selling scenario also had an optimized number of dwellings to fulfill in its design variables, let's compare the current scenario with this one (Table 6.9).

	μ_{LCOX} **range**	σ_{LCOX} **range**
Scenario 2: selling	[619-834]	[103-162]
Current scenario	[619-854]	[105-165]

Table 6.9: Comparison between selling scenario and current scenario.

No notable variation is observed concerning the LCOX range, both for mean value and standard deviation values. This could be explained assuming both that the

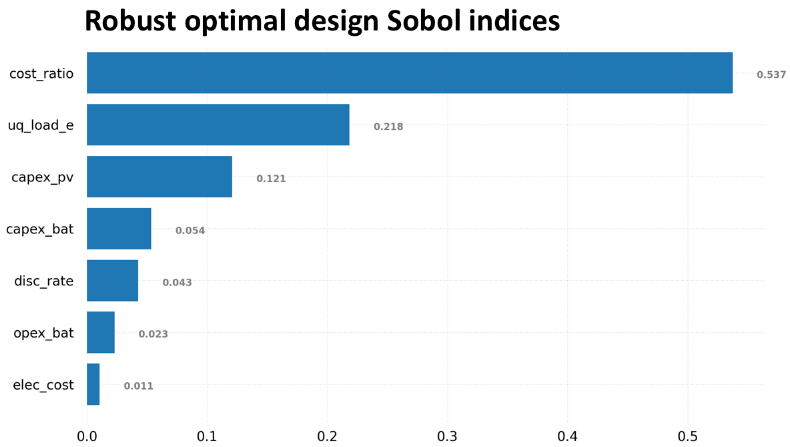

Figure 6.13: 4,4 HP-unit for one load, robust design Sobol indices.
The importance of the uncertain *cost ratio* parameter has been lowered as the design relies significantly less on the grid electricity. The factor *uq-load-e* adapting the electrical demand has a significant impact as it will fix the costly deployment of PV-battery system, also subject to significant cost uncertainties.

optimizer reacts linearly to the number of loads to fulfill and that the installations will follow a very similar configuration. It leads to an equivalent LCOX. The assumed conclusion is that if one may play on the number of dwellings, the optimizer will proportionally adapt to the heat pump nominal power and thus develop proportional power installations.
However, some distinctions can be made between the response in front of uncertainties.

6.5.5 Optimal designs and robust sensitivity

The following Table 6.10 exposes the two optimal designs. The optimizer adapts the design variable n_{load} to match heat pump production and take advantage of it. It leads to enhance the number of dwelling from 1.45 to 2.3 loads. The surrounding electrical installations are also enhanced. The classical scheme is observed:

- The lower mean design relies on pv-panels field but do not consider expensive battery stacks.
- The robustness in the robust design is provided by enhancing PV-fiels and inserting battery stacks to be more self-sufficient.

However, even if the LCOX is similar due to an assumed proportional reaction from the optimizer (LCOX≃cost of installations / exergetic load to fulfill), the Sobol indices of the optimal designs from the current scenario and the selling scenario are not similar.

	n_{PV} [kWp]	n_{bat} [kWh]	n_{hp} [kWe]	n_{load}	μ_{LCOX}	σ_{LCOX}
mean optimal design	23.64	0.04	**4.4**	2.28	624.6	159.5
robust optimal design	37.66	24.52	**4.4**	1.45	837.2	105.2

Table 6.10: Characteristics of the mean optimal design and the robust optimal design

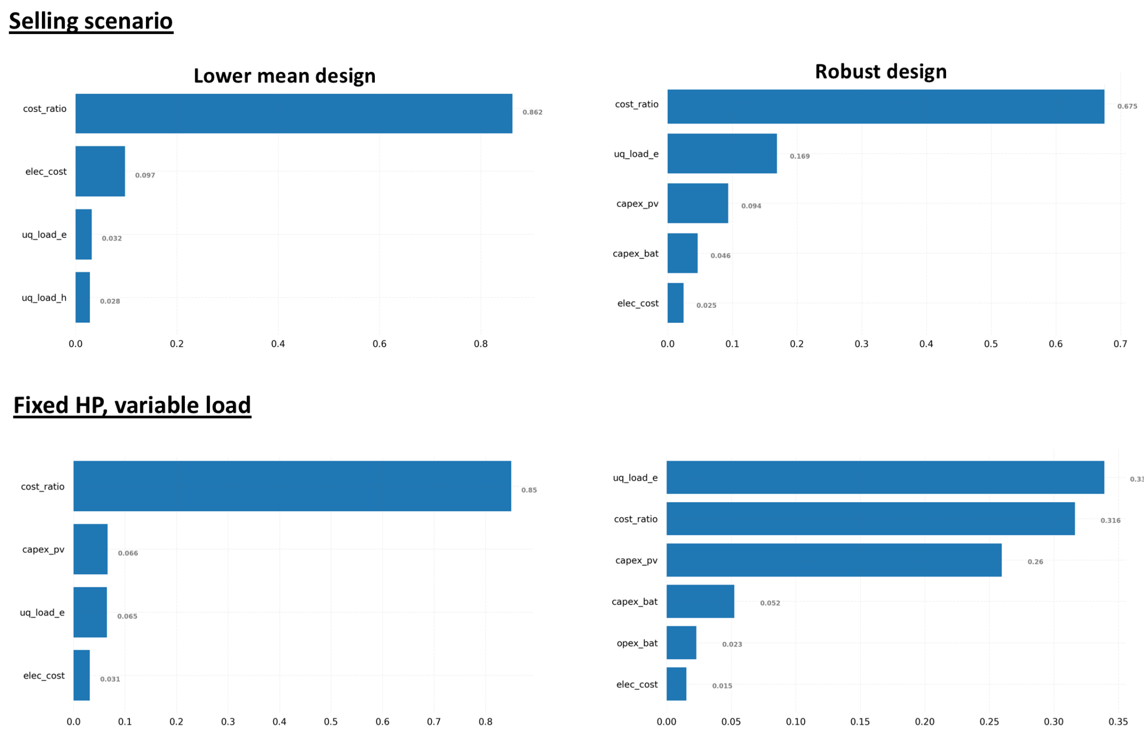

Figure 6.14: Sobol indices comparaison between optimal design from scenario 2 (selling) and current scenario (fixed HP, n_{load} in DVs).

About the **lower mean design** comparison, similar observations can be made. Although, as the fixed HP power scenario requires more PV-panels, the uncertainty on its cost becomes significant.

For the **robust optimal designs** the impact of uncertainties on PV and battery stacks are getting more significant as their installation rises. The uncertainty on the grown load influences the most the stochastic output as it establishes major expensive installations, prone to enhance robustness. On the other hand, as PV-battery couple promotes self-sufficiency, their large deployment in the current scenario reduces even more the impact of *cost ratio* and *electricity price*.

6.6 Summary of HP analysis

The previous analysis exposed that current HP units are not suitable for the load under investigation (scenarios 1 and 2: n_{hp} variable) but are more scaled for loads up to 50% and 120% bigger (scenario 4: n_{hp} fixed, n_{load} variable).

It has been illustrated that oversized units have negative impacts both on mean LCOX and its standard deviation(scenario 3: n_{hp} fixed, $n_{load} = 1$). In fact, the range of use has risen due to the on-off starting security, which leads to more frequent support from less efficient electric boilers. As it claims more electricity, grid electricity is more frequently drawn, at a large uncertain costs. In addition to having paid for an oversized unit, both LCOX objectives are thus worsened.

Chapter 7

Conclusion

The objective of this master thesis is to perform the economic robust design optimization of energy systems including a micro gas turbine, an internal combustion engine and a variable speed heat pump. Those technologies have been paired to PV-battery system on Belgian households. To this end, various uncertainties were taken into account (i.e. gas and electricity prices, loads,...) within a *Python*^{TM} model representing the energy system interactions.
The uncertainties are propagated within the Polynomial Chaos Expansion (PCE) method and NSGA-II algorithm optimizes the global system. The two objectives are minimizing both the LCOX mean value and its standard deviation. In other words, it is lowering the global cost while limiting the impact uncertainties have on it. The interpretation of the optimized results raises assumptions on the economical impact of uncertainties on the system.

Connecting cogeneration units like a **micro gas turbine** and an **internal combustion engine** leads to the same conclusions. When a CHP unit is added to the reference case (PV-BAT-GasBoilers introduced in Chapter 3.1), the optimizer will prefer to reduce the uncertainty on the gas price parameter by downsizing the number of households ($n_{load} \approx 15$). To achieve the robust optimal design, the optimizer shapes designs where the dependency on the grid is lowered by installing PV-battery facilities. In this configuration, more than 90% of the heat demand is covered by the gas boilers. To take advantage of the MGT and ICE units, the gas boilers were replaced by electrical boilers.
In this scenario, the heat demand is mostly covered by the CHP unit and then its pairing to the PV-battery systems becomes more advantageous. However the LCOX standard deviation is much higher than the one of the reference case. The uncertainty on three parameters is responsible for this increase. The gas cost and the parameters related to electricity cost (elec_cost and elec_cost_ratio). Moreover, the LCOX mean value is higher because the installation of a CHP unit for several households is expensive. To take full advantage of this configuration a shared heating network and including heat storage facilities would be interesting. In fact, this way of sharing

heat between consumer would reduce the gas consumption, thus reduce the main uncertainty of the system, the gas cost.
In a future work, more accuracy could be achieved by adding cogeneration policies (green certifications,...) and market conditions in the studied region.

According to our researches, an optimized **heat pump** installation for one load should be around 2 or 3 [kWe]. Unfortunately, the complex unit under analysis (air-water, low temperature, variable speed) does not match existing implementations for such low ranges.
Two studies with a less powerful marketable unit were done (HP unit at 4,4 [kWe] maximal power): the first study for a one-load system, and the second where the load can be optimized. For both, the uncertain parameters related to the heat pump do not weigh in the balance (negligible Sobol indices). As the heat pump is electrically powered, its use enhances the impact of the uncertain price of electricity.
The conclusion for the first study is that an oversized unit has negative impacts for both optimal designs. The impact on the mean value is trivial as a higher price is invested in an oversized installation. Moreover, mean value and standard deviation also get higher as the HP range of working becomes less coherent with heat demand. Back-up electrical boilers, which are less efficient, are more often used, thus, more electricity is required. Therefore, as the electricity price is highly uncertain, it also rises the standard deviation of the LCOX.
The second study (4,4 [kWe] HP to fulfill adaptable load) reveals that the ideal load to minimize the LCOX mean value is 2.3 households. To turn it robust, 1.4 households demands should be fulfilled, with larger PV-battery support. The adaptive load counters the lack of robustness due the oversized unit. In addition, the wider PV-battery deployment decreases the dependency of the system on uncertain grid electricity price.
Future RDO studies including heat pump technology could focus on flat blocks consumption with a powerful shared unit. It may also be interesting to optimize the heat distribution when using at high-temperature air-water heat pump, covering several households equipped by heat storage facilities.

Appendix

NSGA-II

Non-dominated sorting genetic algorithm is one of the best optimizer for exploring and dealing with multiple objectives. The genetic algorithms are based on the sequential evolution of samples population with a modified mating and survival selection. The main idea is to explore many possibilities through mutation of population and taking the best set of them for the next one. The following figure (figure7.1) exposes the main loop of the algorithm, from one population to an optimized one.

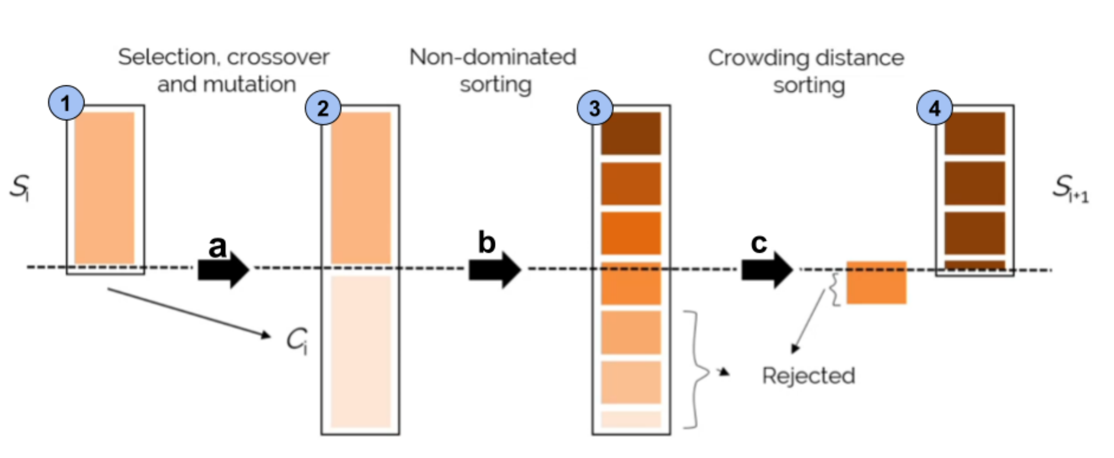

Figure 7.1: NSGA-2 main loop

The different steps and states of nsga-2 loop are:

- State 1: base population S_i of samples (individuals).
- **Step a**: *selection, crossover and mutation*
  A larger population is created (state 2) from the first one, by exploring new design variables (DV). The new set explored is build via mutation (simple actuation of DV) and crossover (combining values from different samples into one).

- **Step b**: *non-dominated sorting*
  The whole new set of samples is then evaluated and the results are non-dominated sorted (state 3). It means that only the best samples are kept, based on Pareto criterion. When no other feasible solution enhances the current one, without worsening other objective functions. The principle is illustrated in the figure 7.2, where the red sample will be rejected because for a same objective function result, other samples enhance an other objective function.

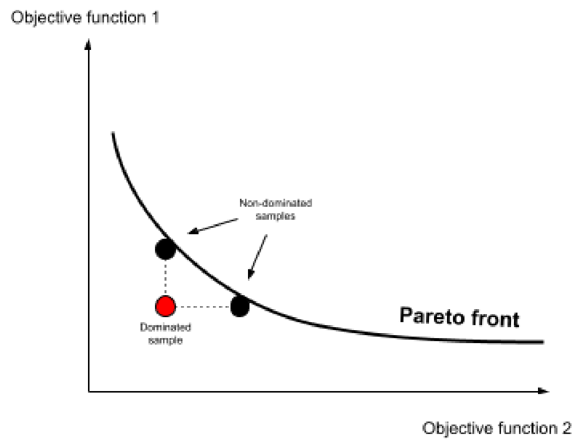

Figure 7.2: Non-dominated sorting algorithm: the red sample is not an optimized one as two other samples provides enhancement for both objective function. It will be rejected from population.
Note that a Pareto front is composed by points, representing one individual design. The curved line is just representative and could be assimilated to a theoretical trend.

- **Step c**: *crowding distance sorting*
  To sort the population down to its initial size, some classification based on "distance" between results is done. It will avoid to keep samples for which the results are too closed and thus enhance exploration. The final and optimal population is then build (state 4) and the process can be repeated to enhance accuracy and exploration.

Bibliography

[1] IEA. *International Energy Agency: Global Energy CO2 Status, report 2019.* [Online; accessed 25-March-2021]. 2019. URL: https://www.iea.org/reports/global-energy-co2-status-report-2019/emissions#abstract.

[2] Hannah Ritchie and Max Roser. *Sector by sector: where do global greenhouse gas emissions come from?* [Online; accessed 25-March-2021]. 2020. URL: https://ourworldindata.org/emissions-by-sector.

[3] Energyville.be. *EnergyVille introduces additional energy system scenarios for electricity provision in Belgium in 2030 and 2050.* [Online; accessed 25-March-2021]. 2020. URL: https://www.energyville.be/en/news-events/energyville-introduces-additional-energy-system-scenarios-electricity-provision-belgium.

[4] Energyville.be. *Battery Pack Prices Cited Below $100/kWh for the First Time in 2020, While Market Average Sits at $137/kWh.* [Online; accessed 25-March-2021]. 2020. URL: https://about.bnef.com/blog/battery-pack-prices-cited-below-100-kwh-for-the-first-time-in-2020-while-market-average-sits-at-137-kwh/.

[5] BloomberENF. *New Energy Outlook 2021.* https://about.bnef.com/new-energy-outlook/. 2021.

[6] Elia. *Electricity scenarios for Belgium towards 2050.* https://www.elia.be/-/media/project/elia/elia-site/electricity-market-and-system---document-library/adequacy---studies/2017/20171114_electricity-scenarios-for-belgium-towards-2050.pdf. 2017.

[7] Géraud Blatman and Bruno Sudret. "Adaptive sparse polynomial chaos expansion based on least angle regression". In: *Journal of Computational Physics* 230.6 (2011), pp. 2345–2367. ISSN: 0021-9991. DOI: https://doi.org/10.1016/j.jcp.2010.12.021. URL: https://www.sciencedirect.com/science/article/pii/S0021999110006856.

[8] Simon Abraham et al. "A robust and efficient stepwise regression method for building sparse polynomial chaos expansions". In: *Journal of Computational Physics* 332 (2017), pp. 461–474. ISSN: 0021-9991. DOI: https://doi.org/

10.1016/j.jcp.2016.12.015. URL: https://www.sciencedirect.com/science/article/pii/S0021999116306684.

[9] M. A. Mikofski W. F. Holmgren C. W. Hansen. "pvlib python: a python package for modeling solar energy systems". In: *The Journal of Open Source Software 3* (2018), p. 884.

[10] W. A. Beckman W. De Soto S. A. Klein. "Improvement and validation of a model for photovoltaic array performance". In: *Solar Energy 80* (2006), pp. 78–88.

[11] P. Hendrick G. de Oliveira e Silva. "Lead–acid batteries coupled with photovoltaics for increased electricity self-sufficiency in households". In: *Applied Energy 178* (2016), pp. 856–867.

[12] I. Colak S. Blaifi S. Moulahoum. "An enhanced dynamic model of battery using genetic algorithm suitable for photovoltaic applications". In: *Applied Energy 169* (2016), pp. 888–898.

[13] S. Syri B. Zakeri. "Electrical energy storage systems: A comparative life cycle cost analysis". In: *Renewable and sustainable energy reviews 42* (2015), pp. 569–596.

[14] T. S. Schmidt B. Battke. "A review and probabilistic model of lifecycle costs of stationary batteries in multiple applications". In: *Renewable and sustainable energy reviews 25* (2013), pp. 240–250.

[15] J. Gomez-Aleixandre G. Diaz. "Maximum income resulting from energy arbitrage by battery systems subject to cycle aging and price uncertainty from a dynamic programming perspective". In: *Energy 156* (2018), pp. 647–660.

[16] L. Wang C. Phurailatpam B. S. Rajpurohit. "Planning and optimization of autonomous DC microgrids for rural and urban applications in India". In: *Renewable and Sustainable Energy Reviews 82* (2018), pp. 194–204.

[17] M. Radzi M. Taghvaee. "A current and future study on non-isolated DC–DC converters for photovoltaic applications". In: *Renewable and sustainable energy reviews 17* (2013), pp. 216–227.

[18] Jayashree Angadi C. M. Harsha. "High Performance DC-DC Converter for Low Voltage Standalone Solar PV Systems". In: *IEEE* (2017), pp. 50–54.

[19] Maurizio Di Paolo Emilio. *AC/DC converters improve power efficiency.* [Online; accessed 11-March-2021]. 2020. URL: https://www.powerelectronicsnews.com/ac-dc-converters-improve-power-efficiency/.

[20] S. Rahman M. Barma R. Saidur. "A review on boilers energy use, energy savings, and emissions reductions". In: *Renewable and Sustainable Energy Reviews 79* (2017), pp. 970–983.

[21] W. Marion S. Wilcox. “Users manual for TMY3 data sets”. In: *Tech. rep., National Renewable Energy Laboratory Golden* (2008).

[22] Maurizio Di Paolo Emilio. *Open Energy Information, Commercial and Residential Hourly Load Profiles for all TMY3 Locations in the United States*. [Online; accessed 9-February-2021]. 2020. URL: `http://en.openei.org/datasets/dataset/%20commercial-and-residential-hourly-load-profiles-for-all-tmy3-%20locations-in-the-united-states`.

[23] I. R. Sanchez M. Montero Carrero. “ Is There a Future for Small-Scale Cogeneration in Europe ? Economic and Policy Analysis of the Internal Humid Air Turbine Cycles”. In: *Energies 12 (3)* (2019), pp. 1–27.

[24] D. Müller R. Sangi P. M. Martin. “Thermoeconomic analysis of a building heating system”. In: *Energy 111* (2016), pp. 351–363.

[25] S. Syri B. Zakeri. “Electrical energy storage systems: A comparative life cycle cost analysis”. In: *Renewable and sustainable energy reviews 42* (2015), pp. 569–596.

[26] N. Bianco M. Di Somma B. Yan. “Multi-objective design optimization of distributed energy systems through cost and exergy assessments”. In: *Applied Energy 204* (2017), pp. 1299–1316.

[27] Bulex team. *Mode d’emploi ThemaTek24*. [Online; accessed 3-July-2021]. 2014. URL: `https://www.bulex.be/particuliers/produits/thematek-1409.html#downloads`.

[28] Martin Joseph Wauters Pierre. *Installations thermiques motrices. Analyse énergétique et exergétique*. 2nd. Presses universitaires de Louvain, 2011. ISBN: 9782874632648.

[29] Dr. N. Lymberopoulos. “Microturbines and their applications in bio-energy”. In: (2004).

[30] S. Abraham W. de Paepe D. Coppitters. “Robust operational optimizationof of a typical micro gas turbine”. In: *Energy procedia 158* (2019), pp. 5795–5803.

[31] Turbec. *Turbec T100 CHP system Technical description Ver 3*. English. 17 pp. 29 december 2009.

[32] F. EMPHASE Musin. “ Personal Communication”. In: *Mons, Belgium* (2017).

[33] Noren C. Hansen J. Oy G. “ Operational experiences from migro-turbine energy Systems. The OMES project. In Proceedings of the 19th World Energy Congress, Sydney, Australia”. In: (2004).

[34] Paul Peter Urone and Roger Hinrichs. *College Physics*. V4.0. OpenStax, 2012. ISBN: 978-1-938168-04-8.

[35] 2G Cenergy. *Technical Specification Sheet. Natural Gas CHP Module. Patruus Series*. English. 2013.

[36] Lecobel Vaneau. *Towards the end of fuel oil heating in Belgium?* [Online; accessed 5-July-2021]. URL: https://www.lecobel-vaneau.be/en/news/towards-end-fuel-oil-heating-belgium.

[37] Niall Kerr and Mark Winskel. "A Review of Heat Decarbonisation Policies in Europe". In: *ClimateXchange Publications* 332 (2021), pp. 2–3. ISSN: 0021-9991. DOI: http://dx.doi.org/10.7488/era/794. URL: https://www.climatexchange.org.uk/media/4625/cxc-a-review-of-heat-decarbonisation-policies-in-europe-feb-2021.pdf.

[38] Le Vif Trends Tendances. *L'interdiction des chaudières au mazout ou au gaz naturel remise sur la table.* [Online; accessed 5-July-2021]. 2019. URL: https://trends.levif.be/economie/politique-economique/l-interdiction-des-chaudieres-au-mazout-ou-au-gaz-naturel-remise-sur-la-table/article-normal-1176839.html.

[39] Daikin. *Altherma données techniques: unités extérieures ERHQ006-016BAV3.* French. 24 pp. 2017.

[40] Roel De Coninck et al. "Rule-based demand side management of domestic hot water production with heat pumps in zero energy neighbourhoods". In: *Journal of Building Performance Simulation* 7 (Jan. 2013), pp. 1–25. DOI: 10.1080/19401493.2013.801518.

[41] Daikin. *Altherma technical data: ERYQ005-007A, EKHBH007A / EKHBX007A, EKSWW150-300.* English. 36 pp. 2006.

[42] Daikin. *Catalogue chauffage: Applications résidentielles, collectives et tertiaires.* French. 356 pp. 2019.

[43] Karl-Kiên Cao et al. "Expanding the horizons of power-to-heat: Cost assessment for new space heating concepts with Wind Powered Thermal Energy Systems". In: *Energy* 164 (2018), pp. 925–936. ISSN: 0360-5442. DOI: https://doi.org/10.1016/j.energy.2018.08.173. URL: https://www.sciencedirect.com/science/article/pii/S0360544218317092.

[44] Sotirios Karellas, Aris Leontaritis, and Konstantinos Braimakis. "Energetic Investigation of Heat Pumps Efficiency Improvement with the Implementation of an Expansion Machine". In: June 2014.

[45] heating AVS and air conditioning. *Heat Pump Installation Cost 2021.* [Online; accessed 14 July 2021]. 2021. URL: https://avsheatingandair.com/hvac-cost/heat-pump-installation-cost/.

[46] Susie Cagle. *Berkeley became first US city to ban natural gas. Here's what that may mean for the future.* [Online; accessed 5-July-2021]. 2019. URL: https://www.theguardian.com/environment/2019/jul/23/berkeley-natural-gas-ban-environment.

UNIVERSITÉ CATHOLIQUE DE LOUVAIN
École polytechnique de Louvain
Rue Archimède, 1 bte L6.11.01, 1348 Louvain-la-Neuve, Belgique | **www.uclouvain.be/epl**